2017

RELATIVE CROSS TRACK ERROR CALCULATIONS IN ASABE/ISO 12188-2:2012 AND POWER/ENERGY ANALYSIS USING A 20 HP TRACTOR ON A FULLY ELECTRIC DRIVETRAIN

Joseph D. Rounsaville
University of Kentucky, joeyrounsaville@hotmail.com
Digital Object Identifier: https://doi.org/10.13023/ETD.2017.477

STUDENT AGREEMENT:

I represent that my thesis or dissertation and abstract are my original work. Proper attribution has been given to all outside sources. I understand that I am solely responsible for obtaining any needed copyright permissions. I have obtained needed written permission statement(s) from the owner(s) of each third-party copyrighted matter to be included in my work, allowing electronic distribution (if such use is not permitted by the fair use doctrine) which will be submitted to UKnowledge as Additional File.

I hereby grant to The University of Kentucky and its agents the irrevocable, non-exclusive, and royalty-free license to archive and make accessible my work in whole or in part in all forms of media, now or hereafter known. I agree that the document mentioned above may be made available immediately for worldwide access unless an embargo applies.

I retain all other ownership rights to the copyright of my work. I also retain the right to use in future works (such as articles or books) all or part of my work. I understand that I am free to register the copyright to my work.

REVIEW, APPROVAL AND ACCEPTANCE

The document mentioned above has been reviewed and accepted by the student's advisor, on behalf of the advisory committee, and by the Director of Graduate Studies (DGS), on behalf of the program; we verify that this is the final, approved version of the student's thesis including all changes required by the advisory committee. The undersigned agree to abide by the statements above.

Joseph D. Rounsaville, Student

Dr. Joseph Dvorak, Major Professor

Dr. Donald G. Colliver, Director of Graduate Studies

RELATIVE CROSS TRACK ERROR CALCULATIONS IN ASABE/ISO 12188-2:2012 AND POWER/ENERGY ANALYSIS USING A 20 HP TRACTOR ON A FULLY ELECTRIC DRIVETRAIN

DISSERTATION

A dissertation submitted in partial fulfillment of the
requirements for the degree of Doctor of Philosophy in the
College of Engineering
at the University of Kentucky

By
Joseph D. Rounsaville
Lexington, Kentucky

Co-Directors: Dr. Joseph Dvorak, Assistant Professor of Biosystems & Agricultural Engineering
and: Dr. Michael Montross, Professor of Biosystems & Agricultural Engineering
Lexington, Kentucky

2017

ABSTRACT OF DISSERTATION

RELATIVE CROSS TRACK ERROR CALCULATIONS IN ASABE/ISO 12188-2:2012 AND POWER/ENERGY ANALYSIS USING A 20 HP TRACTOR ON A FULLY ELECTRIC DRIVETRAIN

ASABE/ISO Standard 12188-2 provides test procedures for positioning and guidance systems in agricultural vehicles during straight and level travel. The standard provides excellent descriptions of test procedures, however it does not provide detail on methods to carry out the calculations necessary to calculate relative cross-track error (XTE), which is the primary measurement used to judge accuracy of the system. The standard was used to estimate the guidance accuracy of a relatively low-accuracy vehicle at 1.25 and 0.5 m s^{-1}. At 1.25 m s^{-1}, a nearest point calculation overestimated mean XTE by 0.8 cm, or 8.2%. The location sampling density was much higher with a 0.5 m s^{-1} travel speed, and mean XTE was only overestimated by 0.1 cm with the nearest point method.

Power and energy data were recorded using a sled with a known weight to vary the drawbar force on asphalt. This will allow a comparison between the electric and conventional tractor over a range of forces applicable to a 20 HP tractor. The electric tractor was found to consume less than half the energy compared to a Kubota L5030 in a common configuration and a custom configuration to match the weight distribution of the electric tractor.

Finger weeding tasks were recorded throughout the year capturing the duration and frequency of these tasks at the University of Kentucky (UK) consumer supported agriculture (CSA) farm. Power and energy data were recorded from the electric tractor while finger weeding. Diesel consumption was also recorded from a conventional tractor while finger weeding. Field data shows that the electric tractor needs approximately 0.532 kWh of energy while a conventional tractor requires approximately 1.258 kWh or energy to finger weed each row of vegetables. Conventional electric bills were compiled

for the University of Kentucky CSA establishing an average monthly electric need. Historic NREL data was compiled establishing an average potential solar resource for central Kentucky. It was determined that a 15 kW photovoltaic array could meet the conventional electric needs of the UK CSA and supply the net energy allowing the electric tractor to meet the finger weeding need.

KEYWORDS: Autonomous, Cross-track error, XTE, Power, Energy

Joseph Rounsaville

05/07/2017

Date

RELATIVE CROSS TRACK ERROR CALCULATIONS IN ASABE/ISO 12188-2:2012 AND POWER/ENERGY ANALYSIS USING A 20 HP TRACTOR ON A FULLY ELECTRIC DRIVETRAIN

By

Joseph D. Rounsaville

Dr. Joseph Dvorak
Co-Director of Dissertation

Dr. Michael Montross
Co-Director of Dissertation

Dr. Donald G. Colliver
Director of Graduate Studies

05/07/2017

DEDICATION

ACKNOWLEDGEMENTS

I would like to say to anyone reading, it is the hope of eternity that fuels every action I take (Luke 12:27-34). If I did not personally know Jesus as my LORD and savior, then indeed my days would be as if I too were chasing the wind (Ecclesiastes 1:18). I understand that my days here are few (James 4:14-17), and it is important for me to keep my eyes on the eternal goal. If anyone would ever like to discuss eternity, or any topic in this paper, please do not hesitate to contact me.

To my wife (Emily) and our family (Pepper, Penny, and little boy soon to be born) – I cherish every moment we get to spend together. It is our time together in the afternoons and evenings that allows me to hold my head up high each morning when I have to leave you for work.

To the Director of my dissertation (Dr. Joseph Dvorak) thank you for taking the risk, stepping outside the box, and bringing me onboard. I have enjoyed our projects together.

To every other UK faculty, staff, and student, I truly do enjoy spending my work day in the environment that each of you help to create.

Thank You!

TABLE OF CONTENTS

LIST OF TABLES

LIST OF FIGURES

LIST OF EQUATIONS

CHAPTER 1: PREFACE AND PROJECT OBJECTIVES

1.1 XTE

A well-documented history exists for the use of automatic vehicle guidance in an agricultural setting (Heraud & Lange, 2009). Currently the use of tractors dominates this usage but new applications are being developed all the time. A few worth mentioning are intercropping (Dybro, 2015), mechanical weeding (Gai, 2015), vineyard management (Rovira-Mas, 2015), scouting (Rains, 2015), and turf mowing (Chang, 2015). The ASABE/ISO 12188-2:2012 standard was developed to quantify the accuracy of an autonomous system.

When an agricultural setting is being discussed, it is common for the vehicle to be driven along a straight line in the field. As such, the ASABE/ISO 12188-2:2012 standard has been created to provide procedures for "testing of satellite-based auto-guidance systems during straight and level travel". Perpendicular deviation becomes quite important while vehicle speed fluctuations account for any parallel deviation and are of less importance.

The cross-track error (XTE) is the calculation commonly used to measure the accuracy of the system and describe the perpendicular deviation (Borhaug & Pettersen, 2005). XTE is defined as the horizontal deviation from the intended travel path. Cross-track error can then be used to describe more complex positional error statistics (Sharp & Yu, 2012). The cross-track error calculation requires a known reference line to describe the intended travel path. However, a known reference line is not convenient in an agricultural setting and this quickly led to the development of the relative cross-track error (XTE). XTE does not require a known reference line and instead uses the difference between two vehicle passes when programmed to drive along the same path. XTE is the primary error measurement in ASABE/ISO 12188-2:2012 and is defined as the "lateral deviation of the Representative Vehicle Point (RVP) from the desired path determined from the previous paths of the RVP when guided along the same test course" (ISO/ASABE, 2012). Being a relative calculation, any systematic bias errors in the data could be missed by techniques of this kind. The standard does an excellent job of outlining procedures for the tests. However, details are not given on how to carry out the calculations on the data

set to report the errors as defined within the standard. A technique will be demonstrated that clarifies and improves the XTE calculation.

1.2 Power / Energy Analysis

The debate surrounding organic farming and greenhouse gases is exceedingly complex and ongoing. It has been suggested that organic farming produces less greenhouse gases when compared to conventional systems (Rodale Institue, 2014). Others claim that certified organic farming increases the greenhouse gases emitted (Julius McGee, 2014) as organic production can require additional field work (Williams, 2006). It has also been suggested that a battery powered vehicle would be suitable for light-duty agricultural work (R. Alcock, 1983). It is believed that these light-duty tasks are common for a typical diversified organic vegetable production community supported agriculture (CSA) farm. Could an alternative energy source be coupled with a battery powered electric tractor to dramatically reduce the greenhouse gases from a diversified organic vegetable production CSA? Experiment 2 was designed to quantify the parameters necessary to design such a tractor.

The American Society of Agricultural and Biological Engineers provides standards for terminology (ASABE, Uniform Terminology for Agricultural Machinery Management, 2015), machinery management (ASABE, Agricultural Machinery Management, 2015), and machinery management data (ASABE, Agricultural Machinery Management Data, 2015). These standards provide estimates of power requirements for many different field operations. However, these are average values with large error margins, and they focus on conventional production systems. The equipment used in organic vegetable production is not always covered in the above standards. Furthermore, no information is given how these loads might be distributed within the field in either time or space. Measuring how the power loads are distributed in time and space can be useful in designing a battery that efficiently stores energy. Providing longer operating times naturally requires higher battery capacity, but these larger capacity batteries are also capable of delivering more instantaneous power should it be needed.

The energy requirements are closely connected to the power requirements, as power is the rate at which energy is transferred. The total energy requirement is vital in

determining energy storage and capacity. When the power profile per task is known, one can begin to add up the desired tasks in time and space to see the desired energy profile. Another consideration is the time needed to recharge the batteries. Larger capacity batteries are capable of providing more instantaneous power, however they also take longer to recharge.

In 1987 the Brundtland Commission defined sustainability as "meeting the needs of the present without compromising the ability of future generations to meet their own needs" (World Commission on Environment and Development, 1987) . Given the above definition, solar energy is a sustainable source of energy, whereas fossil fuels are not sustainable sources. The US Department of Energy estimates the total world energy demand is approximately 400 quadrillion ($400 * 10^{15}$) BTU per year (US Energy Information Administration, 2013). Furthermore, solar possibilities could easily meet these energy needs (US Department of Energy, 2006) . This builds a compelling case for solar as a viable alternative energy source to the more conventional fossil fuel sources. However, the requirements for replacing a conventional fossil fuel tractor with a solar sourced battery powered electric tractor are not well understood at this time. How many tasks could this battery powered electric tractor assume from a traditional fossil fuel tractor? How large would the solar electric power system be to maximize the usefulness of the battery powered electric tractor and minimize the greenhouse gases from the organic vegetable production community supported agriculture (CSA) farm?

A power/energy analysis for a battery powered electric tractor with a fully electric drivetrain will provide a transparent view of exactly what electrical power/energy is required for these tasks. Once these key parameters are quantified, it would be possible to begin accurately sizing a battery pack for precision agriculture needs should any farm wish to pursue a sustainable solar solution. Experiment 3 will begin to shed light on these parameters.

1.3 PROJECT OBJECTIVES

The XTE calculation is already important for an array of agricultural and civilian vehicles where a positioning and guidance systems is used. Furthermore, it is easy to envision the role of autonomous systems expanding. This experiment captures the need to

improve upon the current XTE calculation methodology and presents a demonstrated improvement to the XTE calculation.

Hypothesis 1) Interpolating the path between outbound points or a line of best fit decomposition will improve the XTE as compared to the Nearest Point XTE calculation.

Objective 1) *Calculate and compare the XTE as defined in the procedures of ASABE/ISO 12188-2:2012 of an automated guidance system using a nearest point, linear path interpolation, cubic path interpolation, and a line of best fit method.*

If a battery powered electric tractor can be utilized to reduce greenhouse gases for a diversified organic vegetable production CSA, then what are the sizing parameters of such a tractor? Experiment 2 results in parameters identified and formula given for sizing a battery to meet a given need using an electric tractor.

Hypothesis 2) CLARK will consume less than half of the energy compared to the Kubota L5030 (in a common configuration and a custom configuration approximating the weight distribution of CLARK) at four distinct weight points utilizing a weighted sled and a drawbar attachment.

Objective 2)

- *Determine the power and energy requirements for CLARK to pull a weighted sled at four different weight points.*
- *Determine the correlation between required drawbar force and the current drawn out of the battery for the weight point data.*
- *Determine the fuel consumed by the Kubota L5030 in each configuration to pull the weighted sled at the same weight points as CLARK.*

Can a photovoltaic solar power system be utilized to supply the net energy to a fully electric tractor for agricultural use? Experiment 3 provides the formula and methodology that could be used to begin shifting work from a diesel tractor to an electric tractor and supply the net electric energy for the tractor and the farm with an appropriate sized photovoltaic array. Assume the CSA farm consumes approximately 1300 kWh of electricity each month based on past collected electric bills. Assume the electric tractor

uses 30 kWh (375 Ah * 80 V) of electricity each day for 20 days a month totaling 600 kWh of electricity each month. Total monthly electricity usage would be 1900 kWh. Assume 4.2 sun hours on average each day. A standard 200 watt solar panel is approximately 1.6 x 1 m if a physical size estimation is desired.

$$\frac{1900kWh}{month} * \frac{month}{30days} * \frac{1day}{4.2\,peak\_sun\_hours} = 15.08kW \qquad \text{Equation 1-1}$$

Hypothesis 3) A 15kW photovoltaic solar power system can be used to meet the net conventional electric energy needs of a 12 acre diversified organic vegetable production CSA farm and supply the net energy required for CLARK to meet the CSA finger weeding needs.

Objective 3)

- *Determine the monthly electric energy usage of a 12 acre diversified organic vegetable production CSA farm.*
- *Determine the monthly average photovoltaic resource available for central Kentucky.*
- *Determine the finger weeding distribution in time for the CSA.*
- *Determine the power and energy CLARK would require to meet the annual CSA finger weeding needs.*

CHAPTER 2: LITERATURE REVIEW

2.1 AUTONOMOUS VEHICLES IN AGRICULTURE

Autonomous vehicles are used in a variety of tasks to reduce fuel emission and save on labor costs. This is largely driven by the appeal of renewable sources as fossil fuels are thought to contribute to climate change. An autonomous vehicle presents an opportunity to reduce labor costs and switch to a clean energy source at the same time. An improved and detailed algorithm in calculating XTE will be useful for many autonomous systems in agriculture whenever a relative XTE calculation is desired.

An autonomous robotics lawn-mower (Chang, 2015) has been demonstrated. The design of this mower was intended to reduce noise, air pollution, and labor costs when compared to traditional machines. The mower could be operated in either a manual mode or automatic mode. An electric compass and an odometer was employed to provide input for the two electric drive motors. Microcontrollers were used to actually control the drive motors and receive the signals from the ultrasonic sensors. A laser range finder and groups of ultrasonic sensors were used to avoid obstacles. A human machine interface (HMI) was used to interface with the user as well as gather video from a webcam. The HMI was implemented using National Instruments Labview software. It was concluded that the mower was suitable for use on a variety of turfs and the management of fallow land.

A "VineRobot" (Rovira-Mas, 2015) has been developed to perform a non-invasive map of vegetative growth and determine the red grape maturity. The specific goal of this project was to navigate within vine rows autonomously. A stereoscopic vision camera was used to sense surroundings and perform the trajectory search. A PC was utilized to process the video, GPS, and provide a monitor and touchscreen. Visual perception was provided by a binocular stereo camera, the PG Bumblebee manufactured by Point Grey Research Inc. An Arduino Mega microcontroller, in association with Sabertooth Dual 25 amp motor driver cards, was used to control the drive motors and the steering. This vehicle had a total of five motors, one for each wheel and then one for the steering. In was concluded that the behavior was satisfactory for speeds of about 1 km h^{-1}. The behavior was reported to be unstable in the control commands issued above 1 km h^{-1} due to inconsistency between the vision system calculated angles and the steering angle as measured at the wheels.

Another area of increased attention has been weeding. Weed management is a challenge for organic and conventional farmers. The organic farmers tend to focus on the environmental impact of herbicides and operational costs. Conventional farmers tend to focus on operator health, operational costs, and herbicide-resistance species. The primary thought seems to be that automation can help reduce the labor and chemical applied while significantly improving the weed control in the intra-row region. A plant recognition system using the Kinect v2 camera has been developed and demonstrated (Gai, 2015). Both 2D textual data and 3D point cloud data were utilized by this system. The primary objective of the research was to identify and localize the crop plants within the rows. The algorithm used was to remove the background and noise points, detect the ground plane, then extract the localized plant points. Lastly, plant morphology features were used to distinguish the crop from weeds and to classify the crop. Ground detection was reported to work well on flat ground yet have stability issues in selecting the plant on uneven field ground. Plant localization was reported to be sensitive to plant shape, wind, and perform best on short plants. Overall, the author reported that the Kinect v2 appeared to be a promising and reliable camera for future autonomous agricultural robots. It was concluded that performance was acceptable to detect single plants in crop rows.

An Automatic Field Scout (AFS) has also been developed (Rains, 2015). This is a complex system using an autonomous ground vehicle called the red rover. A robotic arm was added for tissue and ground interaction. And, an unmanned aerial system was used to collect data. Processed video would lead to sample collection via the red rover. The rover would collect the sample and return for further investigation to possibly identify the presence of pathogens or nutrient deficiency. A major goal for the project was early detection and improved scouting information. The red rover is a custom built vehicle from West Texas Lee Corp. The rover was modified to meet the conditions presented by an open field were the crops are clearly visible in rows. Power was provided by a Kohler 20 HP gasoline engine. The robotic arm chosen was a MICO from Kinova. The MICO has six degrees of freedom allowing increased flexibility. Each of the six motors has an encoder for precise positioning. The MICO is equipped with two fingers to allow gentle grasping. The MICO is a small arm, with a reach of only 70 cm and a maximum payload of 750 g at full extension. This system had been field tested at the time of writing.

The idea of a small autonomous vehicle has been used to outline an entire crop production system based on relay intercropping (Dybro, 2015). Specifications are given for a constantly roving autonomous vehicle that could handle seeding, spraying, weeding, and crop sensing. This vision is for a small, somewhat slow vehicle that is nearly always in the field. The author speculates that weeds could either be uprooted or severed just below the field surface by the small autonomous vehicle. While weeding, it would then be possible to scout for other crop issues given the correct sensor configuration. If this is the case, then theoretically one could address deficiencies or disease onset at a very early stage. The author proposes a vehicle weighing approximately 25 kg, 0.508 m in length, 0.193 m in width, 0.250 m in height, with 0.0350 m of clearance. It is assumed that knowing the precise seeding map would assist weeding, as this information could help in identifying plants either correctly located or not. The author concludes that such an autonomous vehicle should enable relay intercropping to significantly increase agronomic output as compared to monocropping.

A whole farm economic analysis was done regarding the adoption of auto-steer navigation to access the economic risks and production implications (Jordan M. Shockley, 2011). It was reported sub-meter auto-steer was profitable and the return on investment was larger than the interest rate. However, at the lowest inward drift scenarios then RTK auto-steer was not profitable and the return on investment was lower than the interest rate. It was concluded that auto-steer could have an optimal impact on corn and soybean production practices.

A master-slave system between agricultural vehicles enabling a semi-autonomous slave vehicle to follow a master tractor was developed (Xi Zhang, 2010). It was concluded that challenges lay ahead to determine the appropriate tolerance zone of the autonomous vehicle and the master vehicle. It was also concluded that having a supervisor in the master vehicle was a key safety back-up to their proposed system. It was reported that preliminary results from computer simulation and field tests indicated the slave vehicle could follow the master vehicle satisfactorily.

A commercially available tracked vehicle was modified for autonomous operation in a forest type environment (H.T. Leidenfrost, 2013). The autonomous operation was provided by two hierarchical fuzzy logic controllers. One controller relied upon ultrasonic

echoes and training data while the other added stereoscopic vision and dispensed with the training data. It was concluded that both controllers could reliably navigate forest paths ranging from 229 to 430 m without GPS navigation.

A review describing the current status of the technologies required for autonomous weed control systems has been performed (D.C. Slaughter, 2007). Four core technologies are identified including guidance, detection and identification, precision in-row weed control, and mapping. The primary obstacle identified was that of weed detection and identification. The advantages and disadvantages of machine vision and RTK GPS guidance systems were compared. Machine vision systems usually required a line-of-sight to the crop row, while RTK GPS usually requires a clear sky and reliable signal with a RTK base station. In addition, four types of weed control technologies (mechanical, thermal, chemical, and electrical) were covered. It was reported that recent work with a chemical spray targets weeds within 1 cm of crop plants. The most common error for machine visions systems was reported to be occlusion with poor plant segmentation using natural lighting being next. It was concluded that additional research was required to optimize the current technology to encompass the range of conditions found in commercial agriculture.

2.2 Cross Track Error

The usual guidance accuracy measurement in agriculture for systems during straight and level travel is the cross-track error (Jordan M. Shockley, 2011). The location of the vehicle is recorded as the vehicle moves along a defined path. A perpendicular error can be calculated from these recorded locations and a more accurately known reference line. However, ASBAE/ISO 12188-2: 2012 defines relative cross-track error (XTE) as the preferred guidance accuracy measurement should an absolute reference line be unavailable. XTE is defined in ASABE/ISO 12188-2:2012 as the “lateral deviation of the Representative Vehicle Point (RVP) from the desired path determined from the previous paths of the RVP when guided along the same test course” (ISO/ASABE, 2012). ASABE/ISO 12188-2:2012 also provides procedures to be used for guidance systems in agriculture during straight and level travel. The test calls for an A-B line to be established as the vehicle travels down and back on a straight course. Location measurements of the

autonomously guided vehicle are taken with a rate of at least 10 Hz as the vehicle travels along the A-B line. The RVP is used so that all measurements are consistently taken at the same point. XTE can then be calculated as the difference between the outbound travel path and the return travel path. The standard calls for the experiment to be done at three different speeds, "slow" (0.1 m s^{-1}), "medium" (2.5 m s^{-1}), and "fast" (5.0 m s^{-1}). The standard also calls for different time intervals between the outbound and return paths so that pass-to-pass and long-term accuracy calculations can be made. Excellent test procedures are provided by the standard to evaluate the accuracy of the automated guidance system. However, details are not provided in how to carry out the calculations on the data to actually report the XTE.

The idea of cross-track error can be discussed in a 1D, 2D, or even a 3D context. It has been demonstrated that 1D cross-track error can be used to estimate 2D positional statistics (Sharp & Yu, 2012). The author would calculate 1D cross track error using a nominal path defined on a map. Then, it would be assumed that the horizontal and perpendicular cross-track error statistics were the same. The author does not focus on point-by-point measurements, but does focus on the overall positional statistics. Specifically, a cumulative distribution function (CDF) is used to model the positional accuracy. The author points out that techniques such has this could be used for static, dynamic, non-line-of-sight, and even indoor situations. The author validated the technique using simulated tracking. It was shown that the reconstructed statistics were close to the actual statistics for two typical applications. One of the systems used for verification was an actual Wireless Ad-hoc positioning system that operated in the 5.8 GHz ISM band. Twenty-nine nodes were placed within an office building covering approximately 2,000 square meters. A person walked around a pre-defined path while location was recorded. The cross-track error was then calculated as the minimum perpendicular distance from a recorded point to a straight line segment of the accepted path from the map. An outdoor case was also considered. The Quiktrak system located in Sydney Australia utilizes 14 base stations and operates in the 400 MHz range. A vehicle was driven around a path while the position was recorded. A known reference line was then assumed from a map and cross-track error was calculated.

Cross-track error has been discussed in depth for the marine environment. Here, the three dimensional case of cross-track can be considered. A control strategy has been demonstrated that guarantee's global stability for line of sight trajectories in 3D space (Borhaug & Pettersen, 2005). The author uses a Line-Of-Sight guidance law to reach stability on the desired path where any nonzero forward speed can be utilized. An advantage of Line-Of-Sight guidance is that the path is described by waypoints only, meaning the vehicle's velocity profile is decoupled from the waypoints. The velocity of the vehicle can be controlled without having to compute new waypoints. The author proposes a sliding mode scheme using eigenvalue decomposition to stabilize vehicle travel on the desired path. The author then uses methods to prove the stability of the path. Ultimately, a successful case study was done using the control algorithm on an actual underwater autonomous vehicle. The author also shows that nonlinear cascaded systems theory can be used to separate the overall system stability from the particular controller. This generalizes the results and makes more easily extended to other systems and controllers.

Another marine based application is to use a Line-Of-Sight algorithm to control the yaw torque between waypoints (Petersen & Lefeber, 2001). Two thrusters on the stern of a ship are assumed to deliver the differential action required to produce the yaw torque. A control law is developed to globally stabilize the heading and cross-track error of the ship between waypoints. The definition used for cross-track error by this author is "the shortest distance between the ship and the straight line". This control law was based on intuitive ship behavior and the corresponding actions a helmsman would take to track a straight line between waypoints. This allows for the desired course angle of the ship to be written as a function of the cross-track error. A coordinate system was chosen such that the x-axis points towards the next waypoint and the y-axis represents the sway position of the ship. The author considers trajectories that are non-zero in curvature, meaning the algorithm does not apply to straight lines (yet the path between waypoints is modeled as a straight line). A feedback control law is developed that stabilizes the heading and the cross-track error to zero. The author used Lyapunov analysis and cascaded control theory to show that the heading and cross-track error did indeed stabilize for the overall system anytime the course angle was stabilized.

2.3 Power and Energy Analysis

ASAE EP496.3 FEB2006 (R2015) is intended to provide assistance in determining optimum practices for managing agricultural machinery operations (ASABE, Agricultural Machinery Management, 2015). Useful information is given to assist in making decisions regarding machine power requirements, capacities, cost, selection, and replacement. Tractor performance estimate equations are provided including maximum power performance expected from a two-wheel, rear driven tractor on a level concrete surface including slippage and tractive efficiency estimates. Power requirement estimate equations due to the implement are provided including, drawbar, soil and crop resistance, motion resistance, PTO, hydraulic, and electric power. Field machine performance estimate equations are provided including field efficiency and field capacity. Cost of use guidance is provided including, ownership costs, depreciation, interest, taxes, housing, insurance, operating costs, repair and maintenance, fuel consumption for tractors, fuel consumption for specific operations, and labor costs. Guidance is given for selecting the appropriate machine capacity focusing on an optimum capacity that has accounted for maintenance, timeliness, and the size of the operation. Guidance is also provided on preparing for the replacement of machinery including capital costs as well as repair and maintenance costs. It should also be noted that this standard is intended to be used alongside ASAE D497 and ASAE S495.

ASAE D497.7 MAR2011 (R2015) is intended to provide representative data values of farm machinery operations to assist managers in estimating performance of field machines (ASABE, Agricultural Machinery Management Data, 2015). Tractor performance examples and coefficients are provided allowing the calculation of drawbar performance, motion resistance, motion resistance ratio, net traction, gross traction and tractive efficiency. Specific fuel consumption by volume and oil consumption data are presented. Draft and power requirement data are presented for a draft force calculation including major tillage tools and seeding implements. Draft force is defined as the “force required in the horizontal direction of travel”. An equation is presented that models the draft force and is parameterized by soil texture, three machine parameters, field speed, machine width, and tillage depth. Rotary power data are presented as functional power either at the tractor PTO or the engine on the implement. Draft power should be added to

rotary power to give total power. Machine performance data are provided for specific tasks including field efficiency, field speed, and repair factors. Cost of use data are presented for tractors, harvest equipment, tillage equipment, and miscellaneous equipment. Reliability data are presented by farm size and by specific operation being performed. Timeliness and working days data are given according to the biweekly period of the year and the region being considered.

ASAE S495.1 NOV2005 (R2015) is intended to establish uniform use of machinery management terms (ASABE, Uniform Terminology for Agricultural Machinery Management, 2015). The ASAE Farm Management Committee proposed this document and it was approved by the Power and Machinery Standards Committee. Some of the terms defined for systems analysis include field efficiency, functional efficiency, field capacity, field speed, field time, life of machine, load factor, effective operating width, theoretical operating width, crop production subsystem, crop production system, timeliness, and timeliness coefficient. Terms defined that are associated with economics include cost accounting, accumulated average cost, custom cost, operating costs, ownership costs, actual depreciation, estimated depreciation, straight line depreciation, lease, obsolete, gross, and net. Mechanical terms defined include breakdown, continuous duty, fuel consumption, major overhaul, and repair.

In a paper written by Alcock, a model was developed that attempted to predict the performance of a battery powered vehicle (R. Alcock, 1983). The author predicts that a lead-acid battery will represent the best possible battery powered source for the near future. However, these batteries are sensitive to an increase in load level. As the load demand is increased (an increase in current required), the available capacity is diminished (decrease in available kWh). The author uses traction prediction equations presented by Wismer and Luth to create a computer model that would predict the energy density requirement of a given field task. The model began by using a range of slip values to determine tractive efficiency and vehicle weight for either a two or four wheel drive configuration. The author assumed a constant battery mass fraction of 0.45 which allowed for the required battery weight to be calculated. Then the algorithm checked to see if the energy density was acceptable for the given battery weight. The author concluded that the energy density for lead-acid batteries was not adequate for energy intensive tasks such as primary tillage.

However, a lower energy task will lengthen the discharge rate and improve the battery efficiency. The author assumed that these batteries are sixty percent efficient given a one hour discharge rate and ninety percent efficient for a three hour discharge rate. The author concluded that a battery powered tractor could be suitable for material handling, seeding, spraying, or light cultivation work. The author stated that power density limitations are not considered in the analysis. Peak power data would need to be obtained then it would be possible to check the ability of the battery to meet peak power demands as well as total energy requirements.

In another paper, Alcock and associates actually measured and tested an electric tractor proposed for chore work (B.P. Thoreson, 1986). The electric tractor that was developed was called the Electric Choremaster I (EC-I). An existing four wheel drive, articulated frame, diesel tractor was converted to be battery powered. The final configuration weight of EC-I was reported to be 5890 kg. The author reported a maximum of 12.2 kW of power available when the hydraulic pump was connected. As the PTO and the hydraulic pump were operated via the same electric motor, connecting the hydraulic pump lowered the available PTO power. The author reported that at this maximum, the battery supplied 19.6 kW, at 155.6 A, being 77.2 percent efficient, resulting in 197.1 Nm of torque. The PTO could be operated for 104 minutes, while these maximum values were not sustainable for the entire 104 minutes. The author reported a maximum drawbar power of 29.00 kW in first at 0.8 m/s, 31.64 kW in second gear at 1.7 m s^{-1}, and 37.73 kW in third gear at 2.6 m s^{-1}. While in second gear, a maximum drawbar pull of 33.2 kN, with efficiency of 54.3 percent, and a slip of 10.05 were reported. The EC-I used series wound DC electric motors. The efficiency of these motors decreases as the speed of the motor decreases. The author reported that for every repeat test, the maximum developed power was always less than the first test. Meaning, as the battery discharged over time then the maximum achievable power also decreased as would be expected. It was reported that the current draw from the battery increased linearly as the drawbar pull increased. The author also developed a model to predict the energy required for a few specific tasks around the farm, including moving snow, loading hay, loading silage, and driving uphill. It was reported that the EC-I could move snow for 3 to 4 hours on a single charge.

The capabilities of different hypothetical designs for electric vehicle in agriculture are discussed with advantages and disadvantages studies (N. L. Buck, 1983). It was concluded at the time of the study that current lead-acid batteries had little or no usefulness on the farm. The power-to-weight ratio was unsuited for most agricultural tasks. It was also concluded that advanced batteries would be suited for hauling and utility tasks. It was also concluded that electric cables are potentially well suited for field tasks because of their high power-to-weight ratio. The obvious obstacle is the expense of the power lines and a way to control the cable itself.

The utility of an electric motor and gasoline engine car coupled with solar cells was evaluated (K. Sasaki, 1997). It was concluded that this hybrid car was practical for driving in urban areas were accelerating and decelerating were repetitious. The authors concluded that the total electric energy consumed in one day by the car could be provided by a 1.6 kW solar array which could be mounted on the roofs of houses or parking lots.

A comprehensive electrical battery model has been proposed and implemented in a Cadence environment (Min Chen, 2006). It was concluded that the dynamic characteristics of a battery (including open-circuit voltage, current, temperature, cycle number, storage time dependent capacity, and transient response) were accurately modeled. A simplified model ignoring self-discharge, cycle number, and temperature was also proposed. The simplified model was validated via comparing Cadence simulation results and data gathered from NiMH (Nickel Metal Hydride) and Li-ion (Lithium ion) batteries. It was reported that the proposed model predicted battery runtime within 0.4% error and the voltage response within 30 mV to any load profile.

A battery model using only the battery State-Of-Charge (SOC) as a state variable avoiding algebraic loop problems has been proposed (Oliver Tremblay, 2007). This model also included a controlled voltage source in series with a resistance. It was concluded that four types of battery chemistry (Lead-acid, Nickel-Cadmium, Lithium-Ion, and Nickel-Metal-Hydride) could be represented by this model. The proposed model required on three points on a discharge curve and was shown to accurately match the discharge curve given by battery manufacturers. The model was validated via simulation curves compared to manufacturer's datasheets.

An electric tractor has been fabricated and tested as an approach to provide conventional agricultural machinery emphasizing zero emission (Weerachai Arjharn, 2001). A 20 kW diesel tractor was converted into a battery powered tractor prototype. The diesel engine was replaced with a 10 kW electric DC motor. The original clutch, flywheel, and transmission were retained from the diesel tractor. A 12 V lead acid battery with 60 Ah capacity was chosen with 10 batteries in series comprising the total battery pack. It was concluded that the electric tractor had an equivalent traction coefficient to the diesel tractor, even though the continuous rated power was lower. An advantage of the DC motor was its ability to handle spikes in the power requirement, although such a sustained power could not be achieved. It was concluded that the overall efficiency of the electric tractor exceeded the diesel tractor even though the original drivetrain was retained from the diesel tractor.

New equations predicting fuel consumption for diesel engines during partial and full loads and under conditions when engine speeds are reduced from full throttle have been reported (R. D. Grisso, 2004). It was stated that Nebraska Tractor Test laboratory (NTTL) reports show an improvement in fuel efficiency over the previous 20 years. This NTTL fuel consumption and power data were analyzed. It was reported that current NTTL data suggest an average annual specific volumetric fuel consumption of 0.213 L kW^{-1} h^{-1} representing a 4.8% decrease compared with the original ASAE EP496.2 estimates.

2.4 Green House Gases and Solar Energy in Agriculture

The debate surrounding how to reduce greenhouse gases in agriculture is ongoing. The Rodale institute has published a report stating that regenerative organic practices reduce greenhouse gases as compared to conventional practices (Rodale Institue, 2014). It is reported that organic practices reduce the energy input from 4,568 down to 3,264 MJ $acre^{-1}$ yr^{-1}, reduce the greenhouse gases from 1,400 down to 906 lb CO_2 $acre^{-1}$ yr^{-1}, and maintain approximately the same yields. Two of the biggest discussion points in the conversation are NO_2 released from the fertilizer, and CO_2 emissions from the equipment. The Rodale institute addresses each of these topics. It is reported that organic practices do require more machinery usage resulting in approximately twice the CO_2 emissions due to burning diesel as compared to conventional practices. It is also reported that conventional

practices use synthetic fertilizer resulting in approximately twice the N_2O emissions as compared to organic practices. As N_2O is the primary greenhouse gas offender in the agricultural setting, this is a substantial increase. In addition, the synthetic fertilizer production itself has a large emissions that is accounted for only in conventional practices. This analysis was carried farther and the energy required was compared for organic and conventional practices. The same trend was observed, as organic practices do require about twice the diesel as compared to conventional practices. And, the energy required to produce the synthetic fertilizer still drives the conventional energy needs higher than organic needs. The study claims this is clear evidence for new trials designed to study organic versus conventional practices in different climates, soils, and within different farming contexts.

The Environmental and Protection Agency (EPA) has compiled an inventory of U.S. greenhouse gas emissions and sinks (EPA, 2007). Extensive data are presented on greenhouse gas emission broken down by gas and by economic sector. The first thing to note is that the EPA reports that the agricultural sector accounts for approximately 6-7% of the total U.S. greenhouse gas emissions. N_2O from agricultural soils (approximately 2.9% of the total U.S. emissions) and CH_4 (approximately 2.7% of the total U.S. emissions) were the primary greenhouse gas offenders in agriculture. Methane is approximately 20 time more potent than carbon dioxide at trapping heat in the atmosphere and nitrous oxide is approximately 300 times more potent than carbon dioxide. It was reported that approximately 67% of all U.S. N_2O emissions came from soil management practices in agriculture. The emitted N_2O is very sensitive to the amount of N that is applied to the soil whether in the form of synthetic fertilizer or manure. As more fertilizer is used, more nitrogen is being added, and more N_2O can potentially be released. However, it should be pointed out that nitrogen fixation is a normal part of the nitrogen cycle and even uncultivated soil will be releasing some amount of N_2O back into the atmosphere via natural process. CO_2 from fossil fuel combustion in agriculture was only approximately 0.7% of the total U.S. emissions. This means that agriculture only contributes approximately 0.8% of the total CO_2 emission for the U.S.

The National Renewable Energy Laboratory (NREL) has compiled large data sets spanning many types of renewable energy sources. The purpose of the NREL geographic

information systems (GIS) maps is to provide the analyzed data and help determine which energy technologies are possible solutions for a given geographic location. The GIS data presented include biomass, geothermal, hydrogen, wind, and solar maps. In particular, photovoltaic (PV) solar radiation data has been compiled for the years 1998-2005 and presented by month (NREL, 2016). These data capture the average daily total solar resource per given month. The maps provide solar power averages for the United States with a resolution of about 10 kilometers in longitude and latitude that can be used to directly create electricity from the solar energy. The satellite radiation model used to create the 10 km PV maps requires hourly images from geostationary weather satellites, daily snow data, and monthly atmospheric data to calculate the total resource available. Concentrating solar power (CSP) radiation maps are also provided by NREL for 1998-2005. CSP data would be preferred if it were desired to use the sunlight to heat a fluid and create electricity similar to the process of a conventional fossil fuel power plant. NREL also presents PV and CSP data sets for 1985-1991 with a resolution of approximately 40 kilometers in either direction. The maps developed at the 40 km resolution use the climatological solar radiation (CSR) model and require cloud cover and atmospheric data to calculate an average daily resource for a given month.

The World Commission on Environment and Development was formed as a direct consequence of the fall 1983 UN general meeting with a mission to unite countries in pursuing “sustainable development”. This commission defined sustainable development as “development that meets the needs of the present without compromising the ability of future generations to meet their own needs”. The commission saw possibilities for economic growth based on sustaining and expanding environmental resources. They believed such economic growth essential to alleviate worsening poverty in portions of the developing world at that time.

The U.S. Energy Information Administration (EIA) “collects, analyzes, and disseminates independent impartial energy information” (US Energy Information Administration, About EIA, 2017) to promote sound policy making and public awareness regarding the interaction between energy and the modern world. The EIA functions within the U.S. Department of Energy as a statistical and analytical agency. Comprehensive data collection programs cover all energy sources, end uses, and energy flows. The EIA is

independent of approval from any other U.S. government agency releases information daily, weekly, monthly, and annually in the form of reports, data browsers, and maps. The data services offered by the EIA are extensive including a state energy portal, country energy portal, U.S. energy mapping, and electricity data browser and many more tools.

The U.S. Department of Energy stated mission "is to ensure America's security and prosperity by addressing its energy, environmental and nuclear challenges through transformative science and technology solutions" (US Department of Energy, About Energy.gov: Mission, 2017). The DoE takes a leadership role in driving towards clean energy, sustaining the U.S. effort in science and engineering emerging technologies, enhancing nuclear security through defense and environmental efforts, and being the parent organization for the EIA. The DoE also works to keep the electric grid secure by partnering with states to guard against physical and cyber threats. The DoE also operates 17 national laboratories that push the boundaries of scientific knowledge. These labs include Oak Ridge, Fermi, Sandia, and Lawrence Livermore.

CHAPTER 3: RELATIVE XTE CALCULATIONS IN ASABE/ISO 12188-2:2012

3.1 INTRODUCTION

ASABE/ISO 12188-2:2012 states "The horizontal distance between RVP positions, recorded when travelling in opposite directions, shall represent XTE for every discrete portion of the test course segments". The first impression is that such a calculation should be straight forward. However, as the terms "lateral" and "horizontal" are not clearly defined in the XTE context, the details needed to carry out this calculation are not clear. Horizontal or lateral deviations should be defined as perpendicular to an existing line or path. As already mentioned, the data is recorded with a frequency of at least 10Hz for the outbound and return path. Meaning, the data streams nor the standard clearly provide a line or path from with to calculate a horizontal or lateral deviation.

A line or path should be created enabling the lateral or horizontal deviation to be used yielding the XTE calculation. The original A-B line should not be used as error already exists in the measurement of the data points used to create this line. Furthermore, this is probably why a relative cross-track error calculation was chosen by the standard to begin with. The following possible solutions are explored and presented. A simple nearest-neighbor approach could be taken and ignore the terms lateral and horizontal. However, if data points are sparse then parallel deviations could overshadow lateral deviations. The path could be interpolated between points so that XTE is calculated based on this interpolated path. However, choosing an interpolation technique and implementing such an algorithm is more complex. Finally, a line of best could be calculated from the data set. This would allow deviations to be decomposed into a parallel and perpendicular component readily yielding XTE. The assumption here is that the calculated line of best fit does indeed capture the intended travel path (and this should be a reasonable assumption to make).

The following illustration (Figure 3-1) captures the possible error of simply using the nearest neighbor approach. If a sampling rate of 10 Hz is used at the 5 m s^{-1} test speed, then data points could be separated by a maximum of 0.5 m. Assume the vehicle perfectly traced the A-B line for the outbound and return path. If the data points of the outbound

and return paths were perfectly staggered then a maximum separation of 0.25 m could exist. This would yield an XTE of 0.25 m using the nearest neighbor approach even though the return path perfectly traces the outbound path.

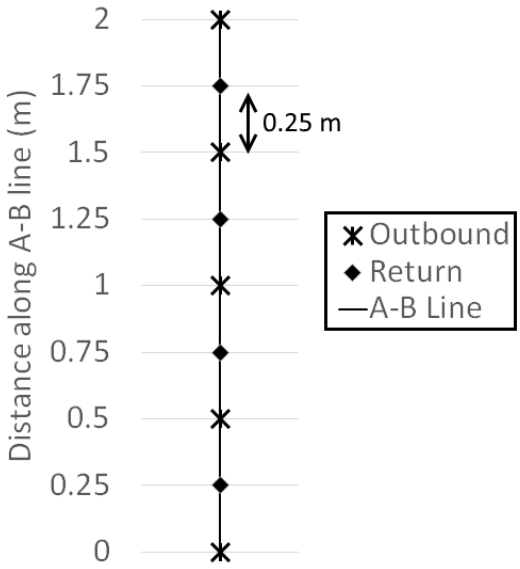

Figure 3-1 Possible XTE of 0.25 m using the nearest neighbor method

A subset of the ASBAE/ISO 12188-2:2012 testing procedure was followed to gather a viable data set using an available fully electric and autonomous tractor. Algorithms were developed so that the data set could be processed using the above mentioned techniques. Differences in magnitude of vehicle accuracy are compared to evaluate the different techniques.

3.2 MATERIALS AND METHODS

The vehicle used for this experiment was a custom built autonomous tractor (Figure 3-2). This particular tractor is often referred to as CLARK. The ground drive and all auxiliary functions were fully electric and operated at a nominal 80 V DC provided by lead-acid batteries and charged when needed by an onboard diesel generator. Navigation and mission control were provided by a Pixhawk autopilot. Location information was provided by a Trimble MS990 which received RTK corrections from the Kentucky CORS network through an NTRIP client. The ground drive consisted of a three phase AC motor

on each rear wheel. Steering was performed with an electric actuator and the three point hitch was operated through an electric over hydraulic connection.

Figure 3-2 Custom autonomous tractor

The electric ground drive consisted of a Zapi DaulAC-2 motor controller (Zapi Group, Poviglio, Reggio Emilia, Italy) and two 7.8 kW Schabmüller TSA240-120-23 AC induction motors (Schabmüller GmbH, Berching, Germany). Each motor was coupled to a PMP S8C.3009.1 gearbox (PMP, Coseano, Italy) to provide a 29:1 reduction and the proper speed range for ground drive. The battery pack was lead acid and was constructed from ten Trojan T875 8 V batteries (Trojan Battery Company, Santa Fe Springs, California, USA) connected in series to produce the 80 V nominal voltage. The complete drivetrain was a series hybrid and included a Polar Power 8340P-40515 diesel generator (Polar Power, Carson, California, USA). This diesel generator integrated a Perkins 404D-15 20 kW diesel engine with a generator, charge controller, and engine accessories necessary for operation, such as the cooling and exhaust packages. The charge controller was configured for operation with the 80 V lead acid battery pack. It utilized the standard multi-stage lead acid charging profile necessary for operation with lead acid batteries. The inclusion of the diesel generator provided the system with the range of a traditional combustion engine system while the electric ground drive (Figure 3-3) facilitated integration with the automation electronics. The motor controllers provided robust, reliable control of the

electric motors and could be configured for a variety of control types. For ease of integration with the autopilot, it was utilized in its speed control mode so that a single speed signal was all that was necessary to properly set the speed of the ground drive.

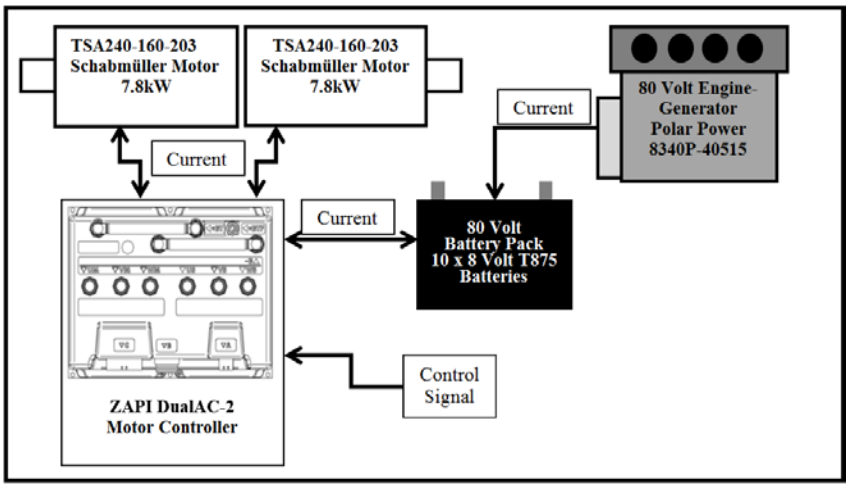

Figure 3-3 Electric ground drive of the custom tractor

The steering was electrically actuated and consisted of a Motion Systems linear actuator, model 85199, (Motion Systems Corporation, Eatontown, New Jersey, USA), a Vex Robotics motor controller, model Victor 888, (Vex Robotics Inc., Greenville, TX, USA), and the steering control code of the main custom control board on the tractor. The steering system integrated position feedback which the control code used to ensure the steering angle was correct. A Meanwell power supply, model SD-1000H-12, (Mean Well USA, INC., Freemont, California, USA) was used to power the electronics and the linear actuator.

The three point hitch was operated hydraulically. The hydraulic power was supplied though a gear pump connected to a Schabmüller TSA200-230-34 AC induction motor (Schabmüller GmbH, Berching, Germany) which was operated by a Zapi FLASH motor controller (Zapi Group, Poviglio, Reggio Emilia, Italy). The hydraulic circuit for the three point hitch consisted of the pump, a tandem center directional control valve, relief valve, two single acting cylinders in parallel, and a flow control valve on the return line to the reservoir. A Celecso string potentiometer, model SP2-12, (Celesco, Chatsworth, California, USA) was attached to the three point hitch so that position of the hitch could be determined. As with the steering, a custom electronics control board

operated the hydraulics that properly positioned the three point based on commands received from the autopilot and mission control system.

The Pixhawk autopilot was an open source software and hardware product. The Pixhawk PX4 (3DR, San Diego, California) used in this study was a high-performance autopilot that specifically targeted research and commercial needs. The PX4 was an evolution of the Ardupilot platform that used an Inertial Measurement Unit (IMU) to determine the vehicle orientation (wiki/Ardupilot, 2016). APM Rover 2.50 was released on June 19, 2015 (diydrones/ardupilot, 2015) and was the firmware version used on the Pixhawk PX4 autopilot for this study. Mission Planner 1.3.31 was released on May 09, 2015 (diydrones/MissionPlanner, 2015) and was the ground control software version used for the guidance accuracy testing. All of the above mentioned were Open Source and freely available.

A Turnigy 9X 2.4 GHz mode 2 radio (Kwun Tong, Hong Kong) was used to control the tractor when the autopilot was not in use. The standard channels of 1 and 3 were used to control the steering and travel speed. An analog knob was chosen for channel 5 to control the three point hitch. The toggle switch was chosen for channel 7 and was configured in Mission Planner to record the current location as a waypoint in "Learn" mode. An analog knob was chosen for Channel 8 and was used to set the operational mode of the tractor. Three operational modes were used in this study (Manual, Learning, and Auto) and were set in Mission Planner.

Two custom printed circuit boards (PCB) were created for this study. One (machine control unit) controlled machine function and integrated the open source 3D Robotics pixhawk autopilot with the custom tractor. The machine control unit used an Arduino Mega2560 (Strambino, Italy) as the micro-controller. The Pixhawk command signals were measured on interrupt lines. These signals follow a standard RC protocol – 5 volt pulse width modulation (PWM) with a high time from 1 millisecond to 2 milliseconds. The period was 20 milliseconds. The machine control unit interpreted command signals for steering, travel speed, and the three point hitch. These commands were combined with the machine status feedback from the embedded sensors in these functions to generate the necessary outputs required for the desired actions.

The second board (the power analysis board) recorded machine power use, location and operating status. This board also used an Arduino Mega2560. This board measured the current flowing into and out of the battery pack as well as the voltage of the battery pack. These measurements were designed to provide detailed information on power requirements. The power analysis board also had an onboard GPS receiver (Ultimate-GPS, Adafruit, New York City, New York, USA) and the ability to receive an additional GPS signal on a dedicated serial bus. In these studies, this connection was used to record the location information provided by the Trimble MS990 to the autopilot. The power measurements and GPS information were recorded to an onboard microSD card.

After building the system, the autopilot had to be calibrated to properly control the tractor. In the Pixhawk autopilot, the travel direction is a very important guidance parameter and can be received via a compass or calculated from GNSS coordinates. When used on UAVs, the compass is the default as they generally run low cost and low accuracy GNSS receivers. For this vehicle, the large metal frame and high power electric motors created magnetic fields that caused erratic operation of the basic compass; however, the GNSS coordinates were RTK corrected and provided an excellent indication of travel direction. Therefore, for this study, the “COMPASS_USE” parameter accessible in the full parameter list was set to calculate the direction from the GPS coordinates.

The Pixhawk autopilot uses a variety of PID loops to control navigation. These PID values were tuned following the procedures given in its documentation ("Tuning steering and navigation for a Rover," 2015) which involved establishing a square test track and continuously operating the vehicle autonomously while adjusting settings until the corners are appropriately followed. The below table (Table 3-1) captures the basic tuning parameters used for this study as set in Mission Planner.

Table 3-1 Steering PID and NAV Parameters.

Steer 2 Servo			Speed 2 Throttle			Throttle 0-100%	
P	3.500		P	0.700		Cruise	50.0
I	0.100		I	0.200		Min	0.000
D	1.000		D	0.200		Max	100.0
INT_MAX	20.0		INT_MAX	40.0		FS Value	910.0
L1 Control - Turn Control			Rover				
Period	17.0		Cruise Speed	2.500			
Damping	0.700		Turn Speed	100.0			
			Turn Distance	15.0			
			WP Radius	0.200			

The guidance accuracy testing was performed at the University of Kentucky campus in Lexington, Kentucky. It was based on a subset of ISO 12188-2. A paved lot was chosen that provided the minimum length of 100 meters in accordance with ISO 12188-2. A line was measured beforehand and desired waypoints were marked (Figure 3-4). The beginning was marked to be waypoint 1. Approximately 24 meters later waypoint 2 was marked. Approximately 110 meters later waypoint 3 was marked. Finally, 18 meters later waypoint 4 was marked. Waypoints 2 and 3 established the A-B line while points 1 and 4 provided a guidance line before reaching the main A-B line to ensure the machine was operating in steady state conditions during the test path as required by the standard. Waypoint 1 was copied as waypoint 8, waypoint 2 was copied as waypoint 7, waypoint 3 was copied as waypoint 6, and waypoint 4 was copied as waypoint 5. The result was waypoint pairs (4 and 5), (3 and 6), (2 and 7), and (1 and 8) that were exact location matches. This created a mission that provided the necessary prior and later travel paths to calculate relative XTE in accordance with ISO 12188-2. The tractor was allowed to drive waypoints 1 through 4 in "AUTO" mode. "Manual" mode was assumed to make the turn then the tractor was allowed to drive waypoints 5 through 8 in "AUTO" mode. The turnaround could have been completed using the autopilot, but using manual control enabled using reverse and changing speeds which improved turnaround time. This ensured that the revisit time was under 15 minutes for all data points as the standard specifies. ISO 12188-2 calls for testing at 5 m s^{-1}, 2.5 m s^{-1}, and 0.1 m s^{-1}, but safety measures implemented during design precluded operating faster than 1.25 m s^{-1}. Therefore, the

system was only tested for target speeds of 2.5 m s^{-1} and 0.1 m s^{-1} with the expectation that the 2.5 m s^{-1} rate would not be reached. The KY CORS corrected GPS data were recorded at 10 Hz also in accordance with ISO-12188-2:2012.

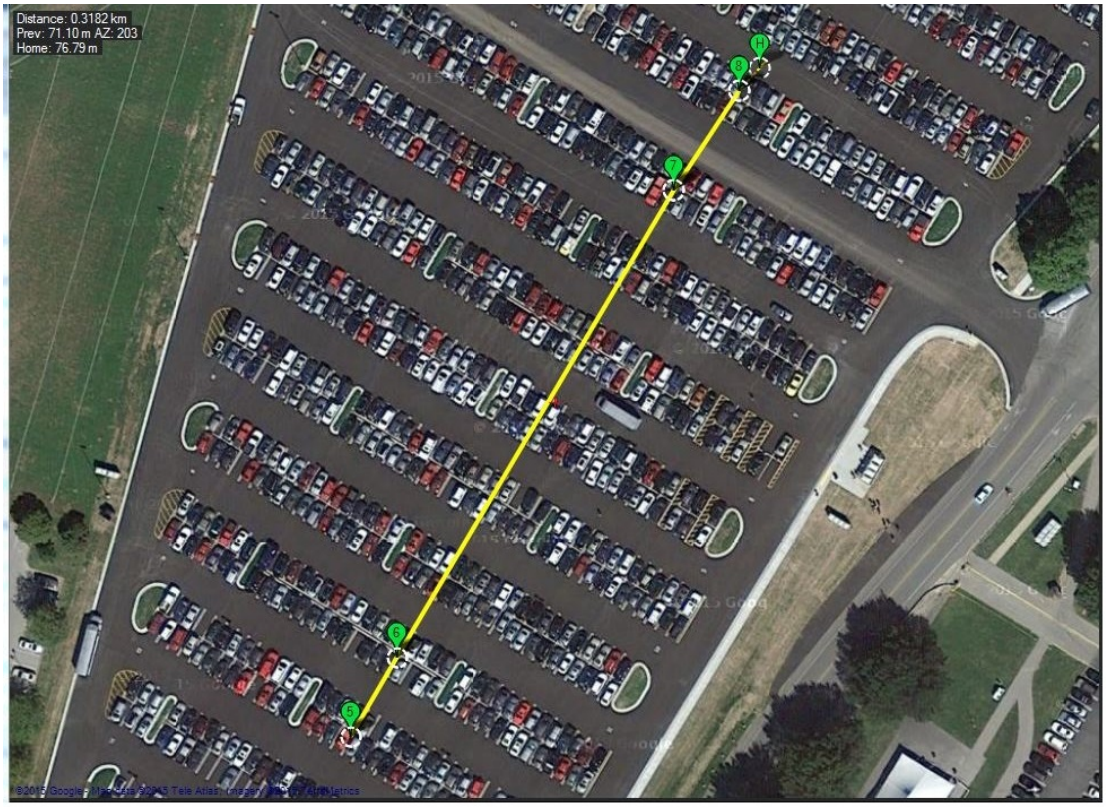

Figure 3-4 Waypoint plan where H represents home

The GPS coordinates for the prior path and the later path were projected into a localized Cartesian (XY) coordinate system with these formula from ISO-12188-1:

$$F_{Lon} = (\cos\phi)\left(\frac{\pi}{180}\right)\left(\frac{a^2}{\left(a^2\cos^2\phi + b^2\cos^2\phi\right)^{\frac{1}{2}}} + h\right) \qquad \text{Equation 3-1}$$

$$F_{Lat} = \left(\frac{\pi}{180}\right)\left(\frac{a^2 b^2}{\left(a^2\cos^2\phi + b^2\cos^2\phi\right)^{\frac{3}{2}}} + h\right) \qquad \text{Equation 3-2}$$

$$\phi = local\_latitude * \left(\frac{\pi}{180}\right)$$ Equation 3-3

Where:

h = average test course height above ellipsoid	33.002 m
a = semi-major axis of ellipsoid	6,378,137 m
b = semi-minor axis of ellipsoid	6,356,752.3142 m
F_{Lon} = location specific conversion factor	
F_{Lat} = location specific conversion factor	
ϕ = location latitude in degrees	

Now, the GPS coordinate data were flattened and brought into a local reference frame:

$$X = (Longitude - ref_{Lon}) * F_{Lon}$$ Equation 3-4

$$Y = (Latitude - ref_{Lat}) * F_{Lat}$$ Equation 3-5

where X and Y were local Cartesian coordinates. Data were analyzed in accordance to ISO 12188-2 which defines positive relative XTE when the later path is right of the prior path. Negative relative XTE is likewise defined when the later path is left of the prior path. ISO 12188-2 clearly defined the XTE; however, implementation details of an algorithm for carrying out the calculation are not given.

3.2.1 Nearest Point (NP) Method

The NP method is the simplest interpretation of the procedure defined by ISO Standard 12188-2 and consists of determining the distance between a point on the return path and the point closest to it on the outbound path. The simplest way to do this is to calculate the distance to every point on the outbound path from every point on the return path. For each point on the return path, the distances are sorted, and the shortest distance is taken as the XTE for that point. This method effectively interprets the term “lateral” from the ISO Standard 12188-2 definition to be the distance to the nearest point on the outbound path. Once appropriate minimum distances are found, the XTE is assigned positive or

negative values depending on whether the return path is to the right or left, respectively, of the outbound path.

3.2.2 Linear Path Interpolation (LPI) Method

The LPI method also requires finding which points are closest to each other between the paths. The LPI method implements "lateral" as interpolating between points on the outbound path to allow a minimum perpendicular distance calculation from a point on the return path to the interpolated segment on the outbound path. As with the nearest point method, this process can be performed using brute force. After presenting the algorithm, the necessity of certain steps will be explained with examples. The following algorithm was developed to calculate XTE by interpolating the paths:

1. **Heading Vector:** As the tractor travels along the return path in questions, a heading vector can be calculated using the previous point and the current point where:

   $R_2 = (X_C, Y_C)$ is the current point on the return path

   $R_1 = (X_P, Y_P)$ is the previous point on the return path:

   $$\xrightarrow[HEADING]{} = (X_C - X_P)\hat{x} + (Y_C - Y_P)\hat{y} \qquad \text{Equation 3-6}$$

2. **Find Points:** In the data, each point on the return path will have a nearest neighbor and a next nearest neighbor on the outbound path. These two points on the outbound path form a line segment where:

   $O_1 = (X_1, Y_1)$ is the point on the outbound path closes to (X_C, Y_C)

   $O_2 = (X_2, Y_2)$ is the neighboring point on the outbound path next closest to (X_C, Y_C).

3. **Form Line:** The two points (O_1, O_2) along the prior (outbound) path form the following line:

   $$ax + by + c = 0 =$$
   $$\left(\frac{Y_2 - Y_1}{X_2 - X_1}\right)x - y + \left(Y_1 - X_1\left(\frac{Y_2 - Y_1}{X_2 - X_1}\right)\right) \qquad \text{Equation 3-7}$$

4. **Calculate (X_M, Y_M):** The minimum perpendicular distance from the above line to (X_C, Y_C) will be at point (X_M, Y_M) where:

   $$X_M = \frac{b(bX_C - aY_C) - ac}{a^2 + b^2} \qquad \text{Equation 3-8}$$

$$Y_M = \frac{a(-bX_C + aY_C) - bc}{a^2 + b^2}$$ Equation 3-9

5. **Check (X_M, Y_M):** If point $O_M = (X_M, Y_M)$ is contained within the line segment O_1O_2, then the point of the relative XTE is $O_{XTE} = (X_{XTE}, Y_{XTE}) = O_M$ and proceed with the algorithm. If (X_M, Y_M) lies outside line segment O_1O_2, then eliminate O_2 as an option and repeat the algorithm from step 2 to find the next nearest point on the outbound path. If no suitable point O_M is found after the desired number of searches, then $(X_{XTE}, Y_{XTE}) = (X_1, Y_1)$ from point O_1. The Euclidean distance between the segment endpoints can be used to determine when O_M is contained within segment O_1O_2 as (Equation 3-10) will be true when O_M is contained within the segment for some multiple of machine precision ($n\varepsilon$):

$$length(O_1O_M) + length(O_MO_2) \le length(O_1O_2) + n\varepsilon$$ Equation 3-10

6. **Magnitude of Relative XTE**: The magnitude of the relative XTE is given as:

$$|XTE| = \sqrt{(X_{XTE} - X_C)^2 + (Y_{XTE} - Y_C)^2}$$ Equation 3-11

7. **XTE vector:** A vector can be defined from the point of the later path to the point of XTE:

$$\underrightarrow{XTEVEC} = (X_{XTE} - X_C)\hat{x} + (Y_{XTE} - Y_C)\hat{y}$$ Equation 3-12

8. **Cross Product:** The cross product between the heading vector and the XTE vector will be purely in the z direction. The sign of this cross product will the sign of the relative XTE:

$$(Z)\hat{z} = cross(\underrightarrow{HEADING}, \underrightarrow{XTEVEC})$$ Equation 3-13

9. **Sign of relative XTE:** The sign of Z indicates the sign of the relative XTE. This determines if the return path was to the right or left of the outbound path:

$$XTE = sign(Z) * |XTE|$$ Equation 3-14

3.2.3 Cubic Path Interpolation (CPI) Method

The CPI method implements "lateral" to be the same as in the LPI method. However, instead of a linear path interpolation, a cubic interpolation is performed. For this analysis, not-a-knot end conditions are assumed. To perform the CPI method, the steps for the LPI

method are used, except that step 4 is replaced with distance measured from the cubic curve rather than the line from LPI. A cubic interpolation provides an interpolation method that assumes a smooth travel path for the vehicle, rather than the disjointed travel assumed by linear interpolation.

3.2.4 Perpendicular Component (PC) Method

The PC method implements "lateral" based on a reference line. The reference line is determined based on a linear regression in the least squares sense on each data set to create a line of best fit (henceforth called *p*). The XTE is calculated from the perpendicular (to *p)* component of a vector defined by the point on the return path in question (R_2) and the nearest point from the outbound path (O_1). The above algorithm and calculations can now be significantly reduced. The need to find the second nearest point, to interpolate between these points to find the minimum XTE, and to do any endpoint check can be eliminated. This simplified algorithm is given below.

1. **X:** Create a vector (X) from the current point on the return path in question and the nearest neighbor on the outbound path where:
   $R_2 = (X_C, Y_C)$ is the current point on the return path;
   $O_1 = (X_1, Y_1)$ is the point on the outbound path closest to (X_C, Y_C).
   $$\overrightarrow{X} = (X_C - X_1)\hat{x} + (Y_C - Y_1)\hat{y}$$ Equation 3-15

2. **P:** Create a vector (P) from the line *p* using any two points such that this vector points in the same direction as the outbound path.
3. **Components:** X has a component parallel to P (the projection of X onto P) and a component perpendicular to P (the rejection of X from P):
   $$\overrightarrow{PROJECTION} = \left(\vec{X} \cdot \frac{\vec{P}}{\left|\vec{P}\right|}\right)\frac{\vec{P}}{\left|\vec{P}\right|}$$ Equation 3-16
   $$\overrightarrow{REJECTION} = \overrightarrow{X} - \overrightarrow{PROEJECTION}$$ Equation 3-17

4. **Cross Product:** As in the previous algorithm, the cross product between X and P will be purely in the z direction. The sign of this cross product will be the sign of the relative XTE:

$$(Z)\hat{z} = cross(\overrightarrow{\ \ }_{X}, \overrightarrow{\ \ }_{P}) \qquad \text{Equation 3-18}$$

5. **Sign of relative XTE:** The sign of Z indicates the sign of the relative XTE. This determines if the return path is to the right or left of the outbound path:

$$XTE_{PC} = sign(Z)^{*}|\overrightarrow{\ \ \ \ \ \ \ \ \ \ }_{REJECTION}| \qquad \text{Equation 3-19}$$

The examples provided below illustrate the LPI and the PC algorithms when used to calculate XTE for point R_2. The outbound path is defined by points O_0, O_1, O_2, O_3, and the vehicle traveled along that path from O_0 to O_3. The later return path is defined by points R_0, R_1, R_2, R_3, and the vehicle traveled from R_0 to R_3. The two points on the prior pass closest to R_2 are O_1 and O_2. Figure 3-5 illustrates a situation in which a steering correction was made on the outbound path also using the LPI method. Because of this, point (X_M, Y_M), lies outside the line segment O_1O_2 and remains outside of any line segment created by the search process. Therefore, from point O_1, (X_{XTE}, Y_{XTE}) = (X_1, Y_1) is used to calculate the XTE. Figure 3-6 illustrates a situation in which point (X_M, Y_M) lies within the line segment using the LPI method. Consider point R_2 of the return path. Points R_1 and R_2 form the heading vector, and point (X_M, Y_M) falls on the line segment O_1O_2. Therefore, (X_{XTE}, Y_{XTE}) = (X_M, Y_M) is used to calculate the relative XTE. Figure 3-7 illustrates the PC method. The magnitude of the perpendicular component of X is the magnitude of the XTE.

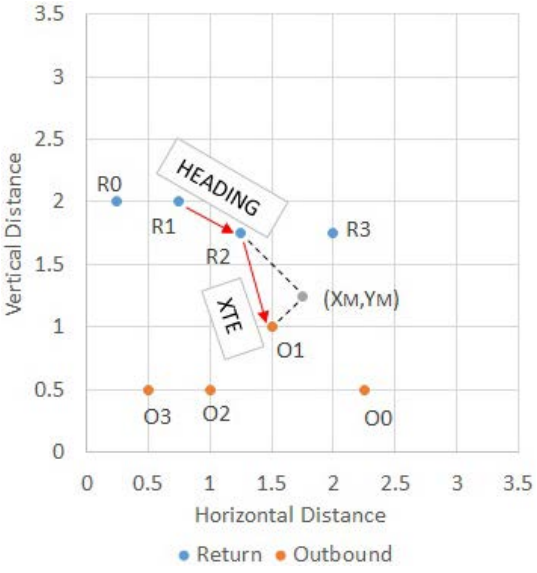

Figure 3-6 LPI method outside O_1O_2

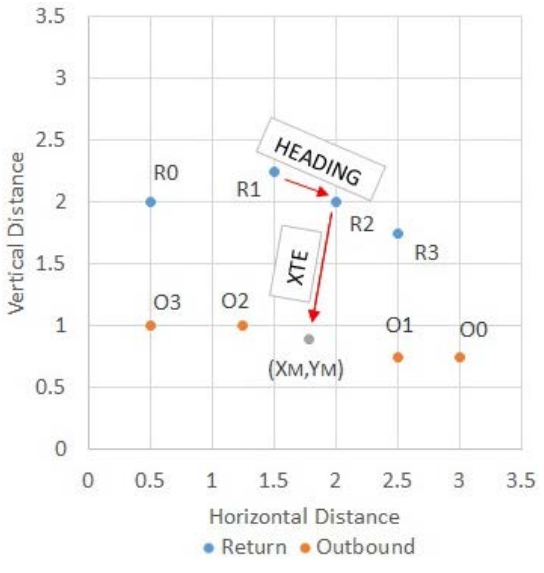

Figure 3-5 LPI method inside O_1O_2

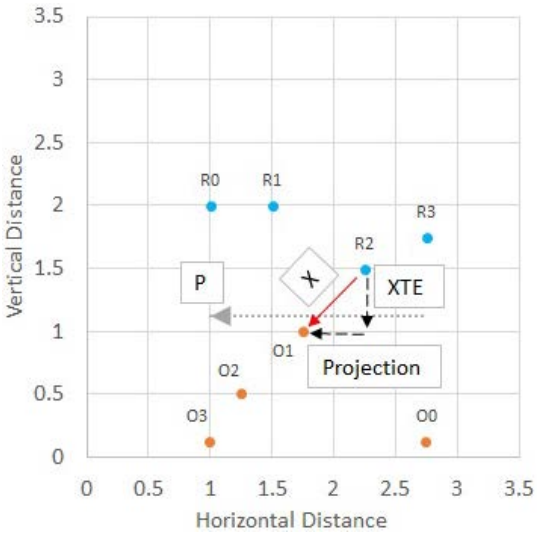

Figure 3-7 PC method

3.3 RESULTS

The simple Pixhawk autopilot was not designed for highly accurate ground travel, so some weaving was noticeable in the travel paths recorded during the test. Figure 3-8 and Figure 3-9 represent the travel paths based on lateral deviation from *p*, which have been rotated to be parallel with the x-axis. These plots show the vehicle position in relation to travel along the return path. Therefore, the vehicle began the out-bound path at the 100 m mark in the plot and traveled until reaching the 0 m mark. It then turned around and traveled back on the return path, starting at 0 m and progressing to 100 m. Noticeable in the plots is lower-frequency weaving and higher-frequency steering corrections present in both test runs. In the run at 0.5 m^{-1}, the low-frequency weaving has a period of approximately 10 m, while at a travel speed of 1.25 m^{-1} the period is between 20 to 30 m. The higher-frequency corrections are most noticeable when they occurred at a peak or valley of the lower-frequency oscillations, but they can be seen at other locations as well. Although all tests (outbound and return and at both speeds) used the same guidance line, the vehicle constantly traveled slightly to the left of the line, generating an offset between the outbound and return paths in both tests. The large deviation at approximately 100 m captures the vehicle settling on the A-B line to begin the outbound path. Finally, the

location sampling was constant at 10 Hz, so at the slower travel speed there is a noticeably greater density of sampling points. Overall, these characteristics created a complicated but realistic set of paths with which to calculate XTE.

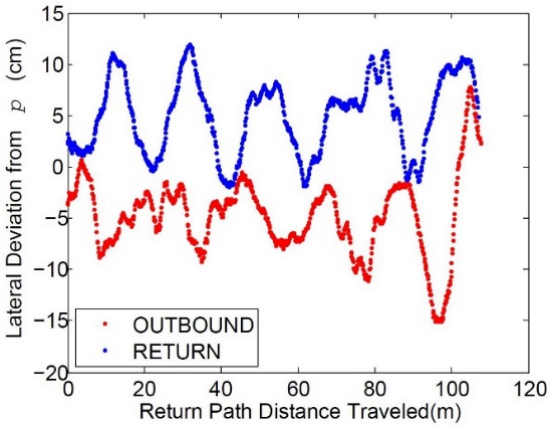

Figure 3-9 1.25 m s^{-1} paths

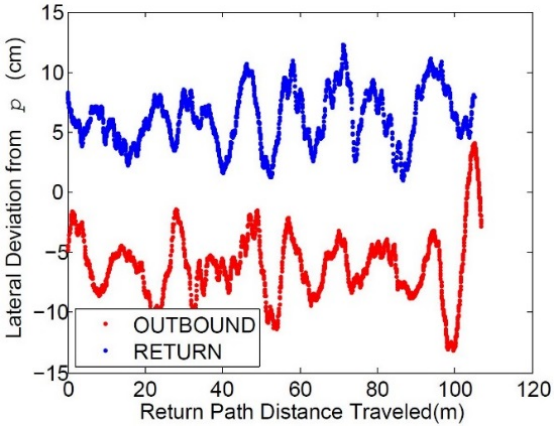

Figure 3-8 0.5 m s^{-1} paths

When comparing the mean XTE calculated using each method (Table 3-2), it is apparent that the NP method performed very differently from the other three methods, and that PC, CPI, and LPI perform nearly identically. Travel speed and the resulting difference in density of location measurements affected the differences between NP and the other methods. At the 1.25 m s^{-1} travel rate, mean XTE_{NP} was 0.8 cm (8.2%) larger than the other mean XTE values, but the difference was only 0.1 cm at the 0.5 m s^{-1} travel speed. As a comparison, assuming perfect navigation but staggered position sampling points, as shown in figure 1, the differences would be 6.25 and 2.5 cm for travel at 1.25 and 0.5 m s^{-1}, respectively. The differences observed in the actual experiment are nowhere near these maximum levels; however, this experiment demonstrates that the theoretical weakness of the NP method with sparse location measurements can manifest itself in actual experiments.

Table 3-2 XTE Comparison

	Mean XTE (cm)	
Calculation Technique	At 1.25 m s^{-1}	At 0.5 m s^{-1}
Perpendicular component (PC)	-9.81	-12.33
Linear path interpolation (LPI)	-9.81	-12.34
Cubic path interpolation (CPI)	-9.81	-12.34
Nearest point (NP)	-10.61	-12.44

Plotting the instantaneous XTE as the vehicle traveled along the path (Figure 3-10 and Figure 3-11) shows the variability that exists in the XTE value that is hidden when looking at the single mean value. The weaving that was apparent in the original paths (Figure 3-8 and Figure 3-9) is also noticeable in the plots of XTE calculated using the PC method (Figure 3-10 and Figure 3-11). At both travel speeds, the XTE was always less than 25 cm, but the XTE was constantly changing during vehicle travel. Only XTE_{PC} is shown because the LPI, CPI, and PC methods yielded nearly identical XTE values.

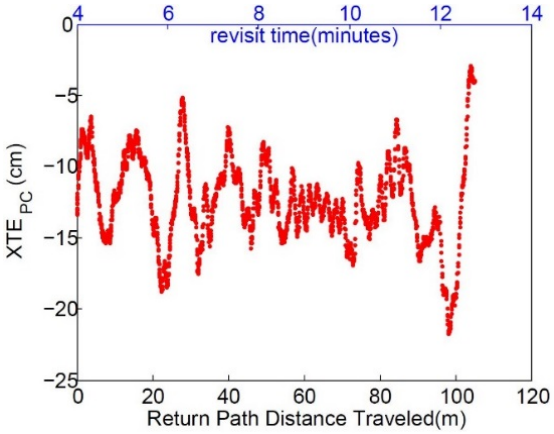

Figure 3-11 XTE_{PC} at 0.5 m s^{-1}

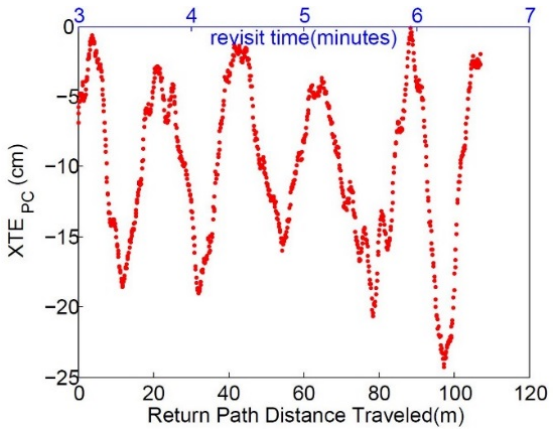

Figure 3-10 XTE_{PC} at 1.25 m s^{-1}

3.3.1 XTE_{NP} and XTE_{PC} Comparison

Just as point XTE varies along the travel path, the difference between the calculation methods can also vary. Figure 3-12 and Figure 3-13 show the difference in magnitudes between XTE_{NP} and XTE_{PC} in each of the guidance experiments. The magnitude of XTE_{NP} was always greater than or equal to the magnitude of XTE_{PC}.

Meaning, the PC method always resulted in an improvement in XTE calculation yielding a positive difference. As expected, the lower sampling density at the higher speed permitted higher differences between calculation methods. The maximum differences were almost 5 cm in the test at 1.25 m s^{-1} but always less than 0.8 cm at 0.5 m s^{-1}. At both speeds, there were certain locations that displayed much higher differences than other locations. At some locations, these differences remained consistent for five or more meters (e.g., peak at 45 m in the 1.25 m s^{-1} test). At other locations with increased differences, some points had increased differences, while other nearby points had almost no difference (e.g., peak at 20 m in the 1.25 m s^{-1} test). Finally, while the average difference between XTE_{NP} and XTE_{PC} was only 0.11 cm at 0.5 m^{-1}, Figure 3-12 and Figure 3-13 show that the point differences were often much larger and that these methods were not as equivalent at this speed as it would seem by only comparing average values.

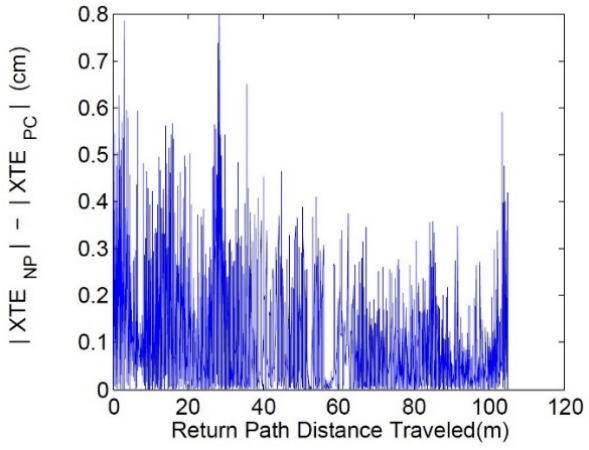

Figure 3-13 $|XTE_{NP}|-|XTE_{PC}|$ at 0.5 m s^{-1}

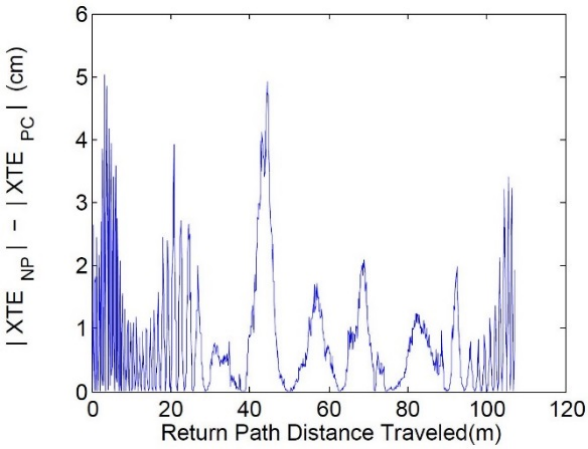

Figure 3-12 $|XTE_{NP}|-|XTE_{PC}|$ at 1.25 m s^{-1}

3.3.2 XTE_{LPI} and XTE_{CPI} Comparison

In contrast to the NP-PC comparison of point XTE values, there was very little difference between the LPI and CPI methods (Figure 3-14 and Figure 3-15). The magnitude of cubic path interpolation XTE (XTE_{CPI}) was very comparable to the magnitude of linear path interpolation XTE (XTE_{LPI}). The differences were all less than 1 mm, and they were distributed above and below zero, indicating little systematic bias. Finally, the differences were spread out throughout the length of the path and were not concentrated in certain locations, as was seen in the differences between NP and PC.

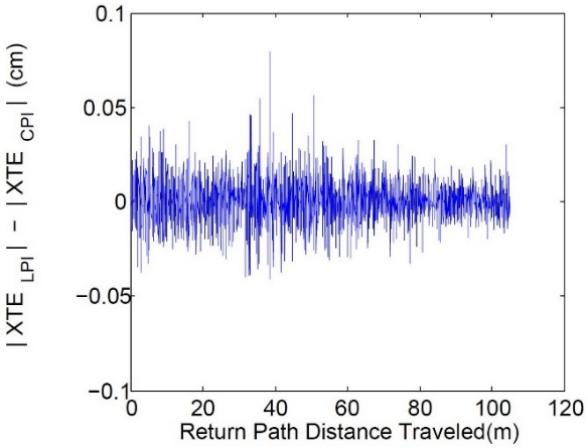

Figure 3-15 $|XTE_{LPI}|$-$|XTE_{CPI}|$ at 0.5 m s^{-1}

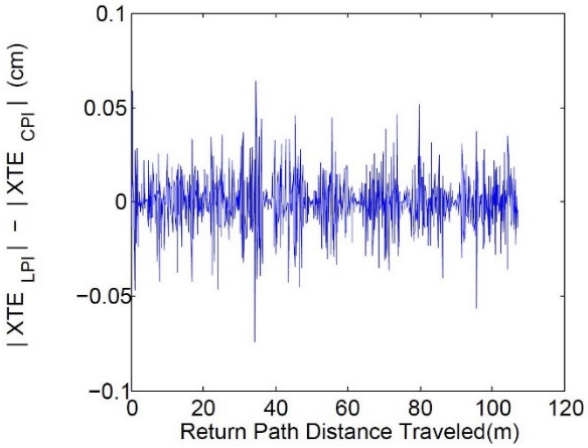

Figure 3-14 $|XTE_{LPI}|$-$|XTE_{CPI}|$ at 1.25 m s^{-1}

3.3.3 XTE_{LPI} and XTE_{PC} Comparison

The differences between XTE_{LPI} and XTE_{PC} (Figure 3-16 and Figure 3-17) were greater than the difference between the two interpolation methods (Figure 3-14 and Figure 3-15), but the differences were always less than 0.5 cm and generally distributed around zero. The differences were evenly distributed in the test at 0.5 m s^{-1}, but there was a slight clustering of errors in the test at 1.25 m s^{-1}. However, this clustering of differences was much less dramatic than that seen in the comparison between NP and PC.

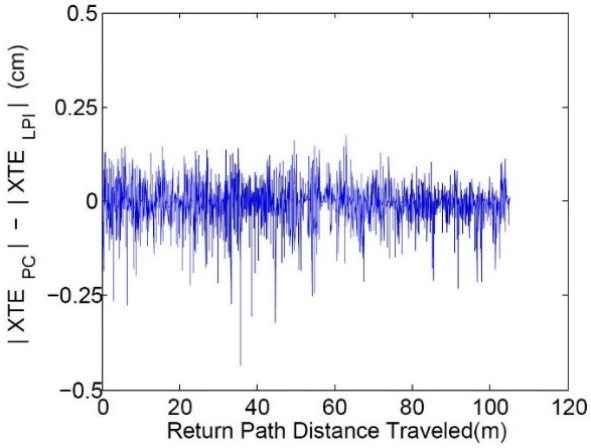

Figure 3-17 $|XTE_{PC}|$-$|XTE_{LPI}|$ at 0.5 m s^{-1}

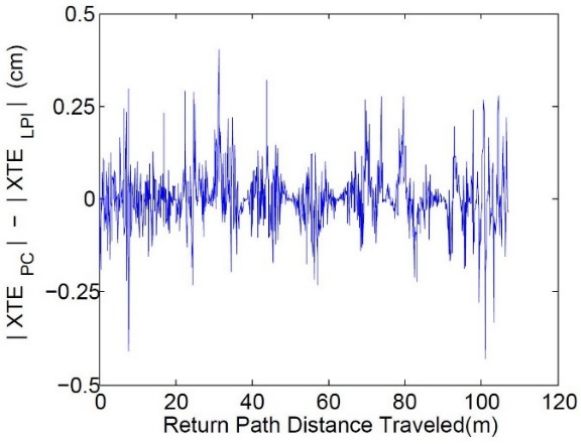

Figure 3-16 $|XTE_{PC}|$-$|XTE_{LPI}|$ at 1.25 m s^{-1}

3.4 DISCUSSIONS

The most apparent result from this work is that the NP method is significantly different from the other methods and appears to overestimate XTE. This difference was illustrated in both the mean XTE values and the point XTE values when they were compared between methods. While XTE_{LPI}, XTE_{CPI}, and XTE_{PC} had small differences between them, which were all distributed around zero, XTE_{NP} was always higher than XTE_{PC}, and these differences were clearly clustered around certain points in the travel path.

Using LPI, CPI, or PC required assumptions about either vehicle travel or an appropriate reference line, but all three methods provided similar results in this testing. Several considerations must be made in determining the most appropriate interpolation method to use. Cubic interpolation provides a smooth connection between all the sample points. With low-acceleration travel, cubic interpolation would be highly appropriate. However, if the travel dynamics include sudden shifts in direction, the cubic interpolation requirement for smooth transitions can result in an interpolated path that extends laterally well beyond the actual travel paths, which could introduce errors in the XTE calculation. On the other hand, linear interpolation assumes straight-line travel between sample points with sudden direction changes at each sample point. This may not capture actual vehicle dynamics, and it cannot interpolate a path that extends laterally beyond the sampled location points. Tractor travel dynamics when performing tillage tasks such as plowing are generally slow and would match the low-acceleration assumption for cubic interpolation. Other tasks, such as high-speed planting and tractor application of liquid or solid inputs, can occur at speeds above 16 km h^{-1}. They can also be performed in no-till ground or in growing crops, where the soil surface is rough, which might not produce the slow dynamics assumed by cubic interpolation. The standard permits testing on "agricultural surfaces" like these. Further, the scope of the standard extends beyond tractors to agricultural ground vehicles in general, so high-speed self-propelled sprayers and even future autonomous equipment that might have travel dynamics very different from those of a plowing tractor should be considered. Because of the wide variety of vehicle dynamics that could be encountered on agricultural vehicles, it is difficult to select one interpolation method over another.

The PC method does not require a specific assumption of vehicle travel dynamics, but it does require a travel reference line from which "lateral" is defined. The application of a relative calculation means that this reference line should be set on the data collected in the experiment. Given this limitation, the most appropriate method to determine a travel reference line is from the best-fit line of the data collected. The standard requires straight-line travel during data collection periods, and using a best-fit line ensures that the entire set of collected data is used in determining the travel path.

One method to limit the differences and improve the accuracy of the simple NP calculation is to ensure that the location measurements are taken at high frequency to generate a dense set of points to describe the vehicle paths. In this testing, this was demonstrated by the much lower mean difference (0.11 cm) between calculation methods when using the more densely sampled paths taken at 0.5 m s^{-1}. It is also possible that the most advanced navigation controls in modern field tractors would exhibit less weaving and produce simpler paths, which might result in smaller differences.

The autopilot for the autonomous vehicle used in this testing was not nearly as refined as those in modern field tractors. However, tractors are not the only agricultural vehicles that are expected to use autonomous navigation. All of the previously cited autonomous agricultural vehicles have unique accuracy levels to achieve success in their applications and will be considerably different from the accuracy of a general-purpose tractor. Some applications, such as intra-row weeding, require the highest possible accuracy, while others, such as automated pre-plant soil sampling, require much lower levels of navigational accuracy. Because of the expected expansion in autonomously guided agricultural vehicles, it is imperative that the standards used for ascertaining accuracy be well-defined, as they could see much wider application than simply on general-purpose tractors. This work demonstrates that a path interpolation or vector decomposition technique, rather than a simple nearest point method, should be used to determine XTE for documenting navigational accuracy.

3.5 CONCLUSIONS

Four different methods have been presented that could be used to calculate XTE from the raw local data that are produced when following the procedures outlined in

ASABE/ISO Standard 12188-2. Three of the methods (LPI, CPI, and PC) produced very similar results, while the NP method provided results that were clearly different. The NP method's strength is the ease with which it can be applied. However, it appears unacceptable for calculating XTE because of its potential to overestimate XTE given the sample rates and speeds required by the standard. Path interpolation, as represented by LPI and CPI, addresses the low density of location measurements by interpolating the vehicle path. The drawbacks of path interpolation are the increased complexity of the calculations and ensuring that the selected interpolation method appropriately reflects the travel of the vehicle in the field. Finally, the PC method produced results very similar to the path interpolation methods, but it required assuming a reference line from the data. This method is relatively simple to implement, but it requires accepting the line of best fit for the travel paths as an appropriate reference from which to determine lateral deviations.

Based on the results of the experiments conducted in this project, there is very little reason to suggest the LPI, CPI, or PC method over the other two methods, as all three methods were reasonable. However, the PC method was simpler to implement in code than the other methods and does not require assumptions on the steadiness, or lack thereof, of agricultural equipment paths. The only additional assumption required of the PC method is that the best-fit line is an acceptable reference line, which would appear to be a reasonable assumption. Based on the simplicity of the PC method and the fact that it varies very little from any path interpolation technique, it appears to be the preferred method for improving the XTE calculation as compared to a simple nearest neighbor method.

CHAPTER 4: POWER AND ENERGY ANALYSIS WITH A WEIGHTED SLED

4.1 INTRODUCTION

Past work has shown that utility type tasks including moving snow, loading silage, and loading hay (B.P. Thoreson, 1986) are suitable for a battery powered tractor. Research also suggests that a hypothetical battery powered vehicle might be suitable for utility tasks such as spraying, seeding, and raking (R. Alcock, 1983). The commonality between these tasks was that they are performed periodically for a shorter amount of time and are not draft intensive.

It is reasonable to ask if an electric tractor could be used for light duty, utility type tasks on a diversified organic vegetable production CSA to help reduce greenhouse gas emissions. If this is possible, then what are the sizing parameters of such a tractor? A power and energy analysis for work done by a battery powered electric tractor with a fully electric drivetrain will provide a transparent view of the electrical power and energy requirements for these tasks based upon empirical data. Once key parameters are quantified, it would be possible to begin accurately sizing a battery pack for precision agriculture needs.

A reproducible and verifiable experiment was designed to collect power, energy, and draft force data over a range suitable for a category 1 tractor. These data were collected for the fully electric tractor alongside data for a Kubota L5030 in a common configuration and a custom configuration intended to match the weight distribution of the electric tractor. The Kubota L5030 was chosen as this tractor is the primary tractor currently used by the University of Kentucky CSA (community supported agriculture) farm for category 1 tasks and is close in size to the electric tractor allowing for reasonable energy comparisons to be made. A model was developed relating the drawbar force to the required electric current for a fully electric tractor.

4.2 MATERIALS AND METHODS

The custom built electric tractor used for this experiment has already been detailed in chapter 3 (Figure 3-2). However, several significant enhancements were implemented before this experiment began (Figure 4-1). The ten Trojan batteries (8 V each) comprising the 80 V pack were removed. The Polar Power diesel generator was also removed. This

freed up space and allowed an 80 V, 375 Ah Crown battery (model# 40-125-11) (Fermont, Ohio) weighing approximately 1,324 kg to be installed. The weather proof enclosures were also relocated to be forward facing on the tractor in version 2.0. The drawbar attachment to the three-point hitch was 31 cm above the ground. The center of the axel was measured at 50 cm above the ground. The drawbar attachment on the three-point hitch was 86 cm behind the axle center.

Figure 4-1 Fully electric autonomous tractor version 2.0

A cooling system for the Zapi motor controllers was designed and installed (Figure 4-2). Custom cooling blocks were machined and placed under each controller. Temperature probes were placed in the fluid flow path as well as on the cooling blocks to determine when to turn on the pump. An Arduino UNO was used as the microcontroller. A Meanwell SD-500H-12 (Fremont, California) DC to DC converter was used to create the 12 V power supply for the pump and electronics from the 80 V battery.

Figure 4-2 Cooling system

A TOTALLIFT TLX80 charger (Clark Material Handling, Lexington, Kentucky) was installed so that the battery could be charged as needed for the experiment. The TLX80 charger (Figure 4-3) was rated at approximately 43 amps given a 208 VAC distribution. The building chosen for installation had an available 208 VAC circuit and was conveniently close to the parking lot chosen for this experiment. The TLX80 charger can perform an equalization charge or a quick charge on the battery. The equalization charge would take approximately four to five hours to complete for the 375 Ah battery. This process is a slower charging process that removes the buildup of lead sulfate crystals from the battery plates. This buildup of crystals will diminish the battery capacity over time. The quick charge for the 375 Ah battery will still take one to two hours depending upon the depth of battery discharge. Performing an equalization charge will store more energy within the battery, but take longer than a quick charge.

Figure 4-3 TotalLift Battery charger

Steps were taken to match the tractive efficiency of the Kubota L5030 to CLARK. Custom wheel centers (Figure 4-4) were designed so that the Samson 9.5-24 rear tires (Canton, Ohio) normally on the autonomous tractor could be mounted onto the Kubota L5030.

Figure 4-4 Custom Wheel centers for the Kubota L5030

Ballasts for the rear wheels (Figure 4-5) were purchased so that the weight distribution of CLARK could be matched by the L5030. Each ballast weighed approximately 48 kg and four were added to each custom wheel center.

Figure 4-5 Custom wheel centers with ballasts

Furthermore, the L5030 was driven in the 2WD configuration. All of these factors mean that the tractive efficiency of the L5030 (Figure 4-6) was intended to match CLARK. The maintenance schedule for the L5030 calls for the air, oil, and fuel filters to be replaced annually. These filters were replaced in March of 2016 and the L5030 was within its regular maintenance schedule. According to the Nebraska Tractor Test report for the Kubota L5030, The center of the axle is 60 cm above the ground. And, the three-point hitch attachment point is 83.6 cm behind the axle. In the common and custom configuration, the height of the three-point hitch was respectively 33.7 cm and 31 cm above the ground.

Figure 4-6 Kubota L5030

A Fuel-View DFM-50C-K fuel flow meter (Nijverheidsstraat, Netherlands) was installed on the injection and return line of the L5030. The fuel meter (Figure 4-7) can measure flow rates from 1 to 50 liters per hour. From this rate, the total liters of fuel that have flowed through the meter are displayed with an accuracy of 0.001 liters. Subtracting the return fuel volume from the injection fuel volume will result in the fuel consumed for a task. When the volume of consumed diesel is known, it is straight forward to calculate the energy consumed (Equation 4-1).

$$X(Liter) * 35.8\left(\frac{MJ}{Liter}\right) * \frac{1}{3.6}\left(\frac{kWh}{MJ}\right) = E(kWh) \qquad \text{Equation 4-1}$$

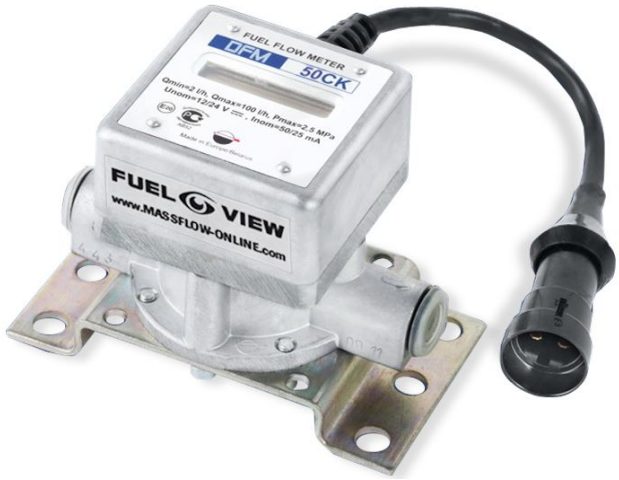

Figure 4-7 Fuel View DFM-50C-K

A weight transfer pulling sled (Figure 4-8) was used to provide a repeatable load. This sled utilized two wooden runners to contact the asphalt (one runner on each side of the sled). This provided a reasonably constant coefficient of friction between the sled and the parking lot. In addition, the weight box was placed in the farthest forward position and the drive chain was then removed from the weight box. Once the sled was moving at a given velocity, the required draft force should also be relatively constant.

Figure 4-8 Pulling sled

With the weight box empty and fully forward, the weight of the sled was recorded as approximately 590 kg total using a tire scale (Figure 4-9) under each wooden runner. The approximate dimensions (Height x Width x Depth) of the sled in meters were 1.6 x 1.8 x 6.7. The chain attached to the frame of the sled just above the wooden runners at approximately 9 cm above the ground. The weight box had room to add 6 concrete weights (Figure 4-10). The weights were approximately a 0.5 m cube weighing 227 kg each. A fork truck was used to load and unload the weights from the sled.

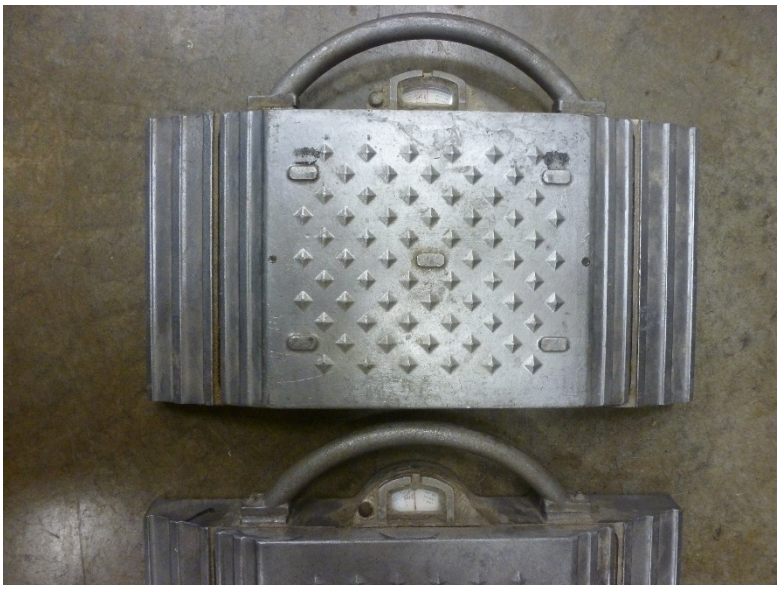

Figure 4-10 Wheel scales with Vernier measurement

Figure 4-9 Concrete weights for the sled

The three tractor configurations utilized in this experiment were CLARK (Table 4-1), the Kubota L5030 as commonly configured (Table 4-2), and the Kubota L5030 custom configuration (Table 4-3). The weight of each wheel and the pressure in each tire was measured.

Table 4-1 CLARK asphalt test

CLARK				
	Left wheel		Right wheel	
	kg	kPa	kg	kPa
Front	363	262	345	303
Rear	708	207	653	207

Table 4-2 Kubota L5030 common configuration asphalt test

Kubota L5030				
	Left wheel		Right wheel	
	kg	kPa	kg	kPa
Front	399	165	426	179
Rear	463	97	463	97

Table 4-3 Kubota L5030 custom configuration asphalt test

Kubota L5030 reconfigured				
	Left wheel		Right wheel	
	kg	kPa	kg	kPa
Front	345	152	363	165
Rear	680	179	685	193

The Kentucky Mesonet is a network of automated weather and climate monitoring stations that is being developed by the Kentucky Climate Center and Western Kentucky University (Kentucky Mesonet, 2017). A mesonet data station is located on the UK CSA at latitude 37.98 degrees and longitude -84.53 degrees. Data gathered from the mesonet included air temperature, relative humidity, precipitation, wind speed, wind direction, and solar radiation. These data are compiled and presented in an assortment of ways. Some data are presented as live data, other data are compiled for hours, days, weeks, or even for the year. The mesonet data were recorded to reflect the atmospheric conditions during the experiment.

4.2.1 Instrumentation

An Omega LCCD-10K S-beam load cell (Norwalk, Connecticut) was chained between the sled and the tractor drawbar to record the draft force. The chain on the sled (84 cm) plus the load cell hardware (91.4 cm) resulted in a hypotenuse length of approximately 1.754 m between the sled and the drawbar. The rated capacity of this load cell is 44,482 N. The Omega load cell (Figure 4-11) produces a differential output voltage on two wires that represent the load across the cell. The load cell was driven at 5 VDC with an output of 3.0 mV/V. This yields a maximum theoretical differential output voltage of 15 mV.

Figure 4-11 Omega LCCD-10K load cell

The differential output voltage from the omega was amplified using a Texas Instruments INA128 instrumentation amplifier (Dallas, Texas). A nice feature of the INA128 (Figure 4-12) is that the gain can be set with a single external resistor. For this

experiment a gain of 100 was chosen by the designer. The gain can be calculated with a single formula (Equation 4-2).

$$G = 1 + \frac{50k\Omega}{R_G}$$ Equation 4-2

This equation can easily be solved for R_G (Equation 4-3).

$$R_G = \frac{50k\Omega}{100 - 1} = 505.05\Omega$$ Equation 4-3

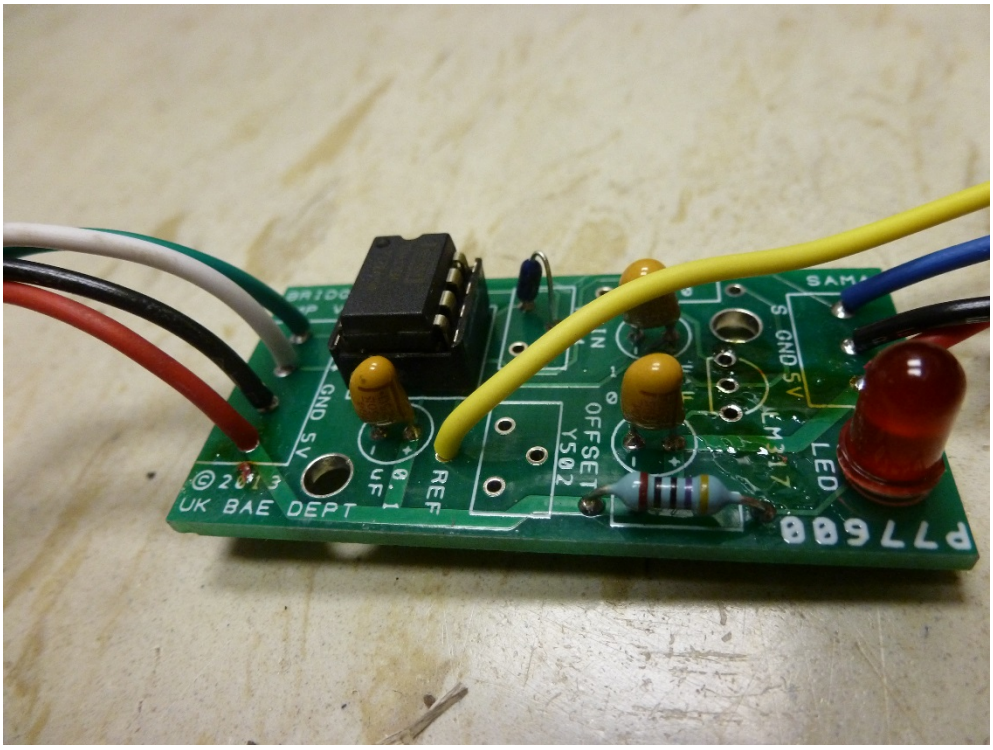

Figure 4-12 Instrumentation amplifier

A precision 505 ohm 0.1% (1/20) watt resistor was chosen by the designer to very precisely set the gain for this experiment. Another nice feature of the INA128 is that a pin is provided to allow an external reference to be set for the differential output voltage. The power analysis board was already using 2.5 VDC as an external reference and this was provided to the INA128.

Combining all of the above, 3 mV/V from the load cell, gain of 100, using a 5 V source, and centered at 2.5 V it was expected that V_{OUT} of the INA128 would range from 1 V to 4 V when expansion and contraction of the load cell are considered (Equation 4-4).

$$\frac{3mV}{V} * 5V * 100 = 1.5V \qquad \text{Equation 4-4}$$

The power analysis board designed for CLARK included a GPS receiver and a micro SD card for data logging (Figure 4-13). The measured force was also displayed onto the serial monitor allowing for a convenient visual inspection if connected to a computer. It was decided to use one of these boards to log the GPS data and the force measurements for CLARK and the L5030 in this experiment. The analog to digital converter (ADC) on the Arduino Mega was a 10-bit ADC, meaning that 2^{10} = 1,024 distinct values can be measured by the ADC over the 0 V to 5 V range. The full scale range of the instrumentation amplifier was 1 V to 4 V spanning 614 distinct levels of the ADC. The load cell range was 0 to 4,536 kg of force for expansion spanning 1.0 V to 2.5 V (or 307 distinct levels of the

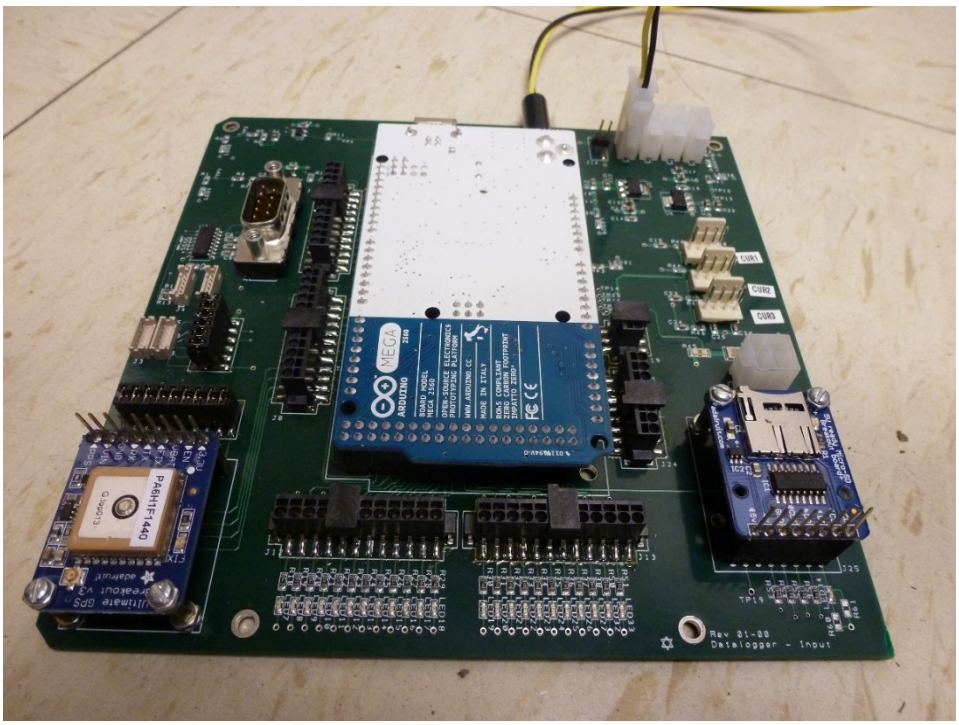

Figure 4-13 Power analysis board

ADC). This all implies that the expected resolution of the system is approximately 14.8 kg of force per ADC level.

The current load out of the battery was measured using a Hall Effect current transducer manufactured by LEM (Figure 4-14). This transducer had a measurement range of ± 900 amps, and this range easily covered the expected currents. A reference voltage of 2.5 V was supplied to the transducer. A small PCB was designed for this transducer to allow convenient placement on the large cables from the Crown battery to the Zapi invertors. The formula for calculating the primary current from the output voltage of the transducer was given in the datasheet and depends on the direction the current flows through the transducer (Equation 4-5). This analog voltage was measured by the Arduino Mega.

$$V_{OUT} = V_{REF} \pm \frac{1.25 * I_P}{600}$$ Equation 4-5

Figure 4-14 LEM HTFS-600P

A voltage divider (Equation 4-6) was used to measure the Crown battery voltage. Again, the Arduino Mega was used to measure this analog voltage. Precision 0.1% resistors were chosen for the below values.

$$V_{BATT\_SENSE} = V_{BATT} * \left(\frac{402\Omega}{402\Omega + 10k\Omega} \right)$$ Equation 4-6

4.2.2 Calibration of the load cell

The load cell was calibrated using a hydraulic press that was setup in the machine systems development lab at the University of Kentucky. The high pressure hydraulic table (Figure 4-15) utilized a fine and a course adjustment dial to apply pressure to the hydraulic press. The table had to be turned "ON", then "armed", and finally the green "Start" button could be pressed.

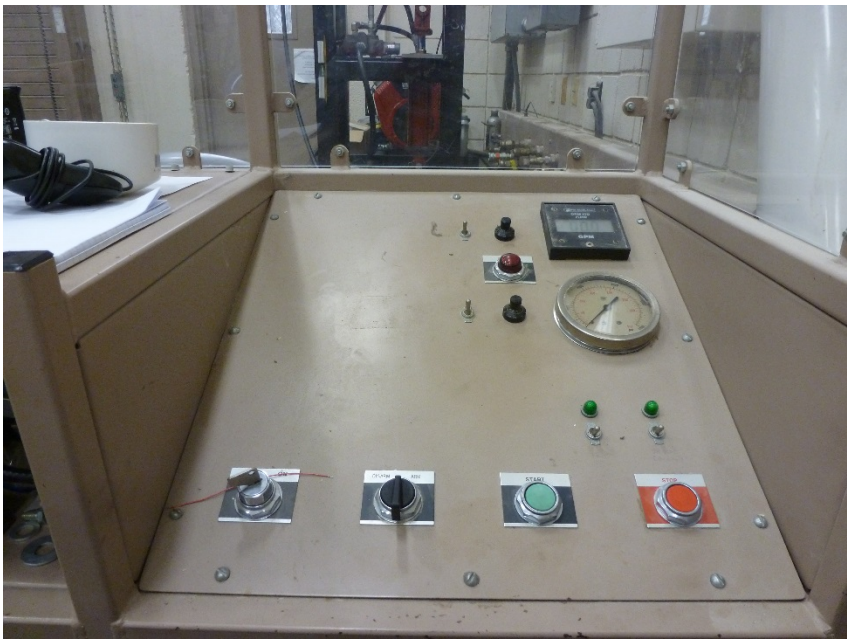

Figure 4-15 Hydraulic press control table

A Cross manufacturing double acting hydraulic cylinder with a threaded rod end was used in the hydraulic press. The rod diameter was 2.9 cm and the bore was 7.6 cm (Figure 4-16). Force was applied by retracting the cylinder to apply a tension load on the load cell. A Cross manufacturing double acting hydraulic cylinder with a threaded rod end was used in the hydraulic press. The rod diameter was 2.9 cm and the bore was 7.6 cm.

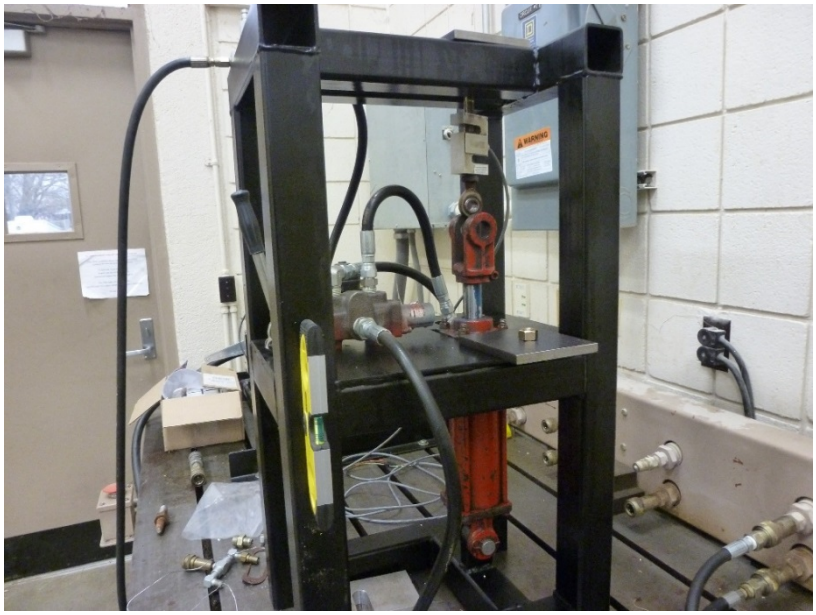

Figure 4-16 Hydraulic Press

The formula for the double acting piston (Equation 4-7) can be applied as follows with force in (N), pressure in (Pa), and area in (m^2).

$$F_{ROD} = (A_{BORE} - A_{ROD})P_{ROD}$$
$$= (\pi * 0.0381^2 - \pi * 0.01429^2)P_{ROD} = 0.003919 * P_{ROD} \qquad \text{Equation 4-7}$$

The pressure was measured using a Fluke 700G30 pressure gauge (Figure 4-17). The gauge has a full scale range of up to 34,474 kPa with a precision of 0.7 kPa.

Figure 4-17 Fluke 700G30 pressure gauge

The Arduino mega, instrumentation amplifier, and the load cell system was set up and measured with the hydraulic press. This allowed a calibration for the entire system to be performed. The hydraulic press was turned on and the Fluke 700G30 was zeroed at 0 kPa. Then the pressure was increased to 827, 2068, 3447, 4440, 5136, 5915, 6936, 7639, 8259, and 9032 kPa which generated forces of 3242, 8104, 13509, 17401, 20128, 23179, 27183, 29936, 32369, and 35394 N as measured by the Fluke 700G30 to calibrate over the entire range of forces expected to be measured for the experiment (Table 4-4). The measured force was read from the Arduino Mega on the serial monitor while the actual force was calculated from the Fluke 700G30 measured pressure (Equation 4-7).

Table 4-4 Load cell calibration data

P(kPa)	$F(N)_{ACTUAL}$ From Eq. 4-7	$\lvert F(N)_{RECORDED} \rvert$ Arduino logged
827	3242	4056
2068	8104	9421
3447	13509	15506
4440	17401	19705
5136	20128	22463
5915	23179	25799
6936	27183	30145
7639	29936	33045
8259	32369	35941
9032	35394	39126

These data were plotted and trend lines were calculated (Figure 4-18). This allowed a convenient way to calibrate the system to known and accurate force values. Any recorded force from the Arduino Mega can be immediately mapped to a precisely known force value.

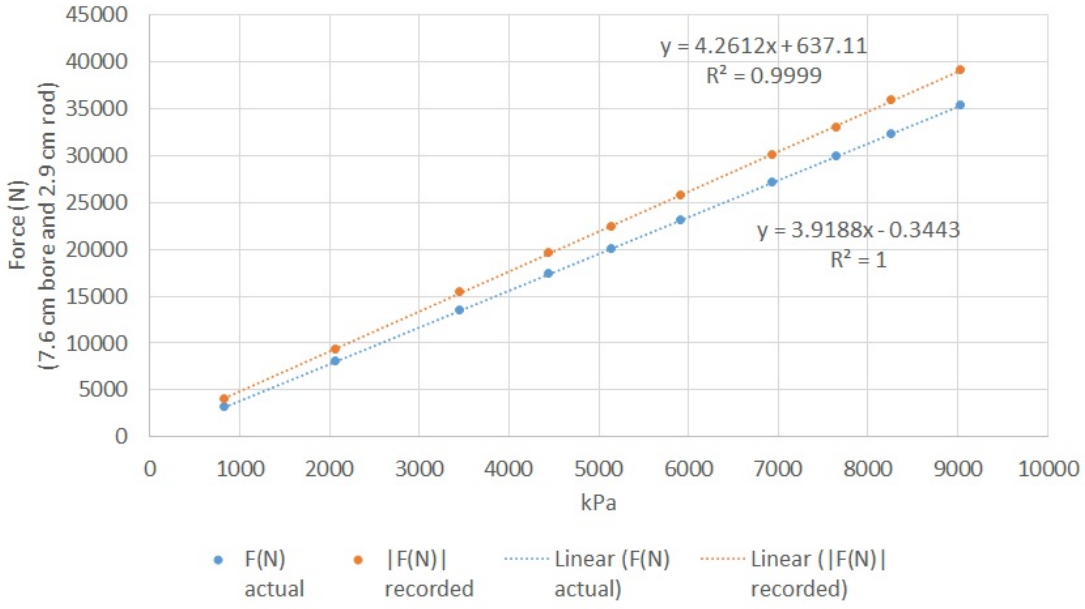

Figure 4-18 Load cell calibration on 18 November 2016

$$F(N)_{RECORDED} = 4.2612 * P(kPa) + 637.11 \qquad \text{Equation 4-8}$$

$$F(N)_{ACTUAL} = 3.9188 * P(kPa) - 0.3443$$ Equation 4-9

$$F(N)_{ACTUAL} = 0.9196 * F(N)_{RECORDED} - 585.572$$ Equation 4-10

4.2.3 Procedures

A large, flat parking lot was chosen for this experiment. Approximately 30.5 m in length was marked off on each side of the parking lot with ample room at each end to turn around. CLARK was driven the 30.5 m pulling the empty sled along one side while data were recorded. Approximate start and stop times were recorded by hand as a check to the GPS data. At the end, CLARK was stopped and backed up approximately a half meter so that the load cell could clearly record the force dropping to zero. CLARK would remain stationary for approximately one minute allowing a clear division in the GPS data so that the desired data could easily be found within the large data set. CLARK made the broad turn and again inserted a pause while also backing up enough to remove all tension from the load cell. CLARK then drove along the other side of the parking lot recording data. This process was repeated for a total of three repetitions representing approximately 91.5 m of data. It was then verified that energy data were recorded for all three repetitions at this weight point. After the file was verified, a single 227 kg block was added to the sled. Three more repetitions were recorded for the second weight point. Another 227 kg block was added and three repetitions were recorded for the third weight point. Finally, another 227 kg block was added and three repetitions were recorded for the fourth weight point. In total, the CLARK data set consisted of four weight points with each having three repetitions. At weight 3 and weight 4, CLARK was unchained from the sled to make the turn at the end of a 30.5 m section of data. A fork truck was used to actually maneuver the sled through the corner. Then, CLARK was chained to the sled again. The large turning radius of CLARK coupled with a heavy sled simply made the turns awkward at the heavy weights.

A very similar process was repeated for the Kubota L5030. The major difference being that energy data were not logged by the Arduino Mega for the Kubota L5030. The Kubota was driven to the 30.5 m section and then backed up and turned off to allow the load cell to drop to zero force. A total fuel flow reading was taken while the Kubota was turned off before the force data were taken. The Kubota was then turned on and driven the 30.5 m while force data were recorded. At the end, the Kubota was backed up approximately a half meter to allow the load cell to drop to zero force and then turned off. A total fuel flow reading was again taken at the end of the 30.5 m section. This allowed a clear measurement of the fuel used in the 30.5 m of data that was taken. It should also be noted that the Kubota L5030 common configuration actually started at the heaviest weight point and removed weight to gather the four weight points (descending in weight instead of ascending in weight like CLARK). This was done simply because upon completion of the CLARK experiment the sled was already loaded with the three concrete blocks and this seemed like a reasonable place to start the second piece of this experiment. The Kubota was driven in the medium gear range with an engine speed target of 1700-1800 RPM for all runs while being in 2WD.

This process was again repeated for the reconfigured Kubota L5030. The reconfigured Kubota L5030 used the custom wheel centers (Figure 4-4) and the additional wheel ballasts (Figure 4-5). This allowed the exact Samson 9.5-24 rear tires from CLARK to be used on the Kubota and for the rear weight distribution to match CLARK. Suitcase weights were removed from the front of the Kubota L5030 so that the front weight distribution also matched CLARK. It should also be mentioned that the reconfigured Kubota L5030 began at the lightest weight point and ascended to the heaviest weight point. This was done because upon completion of the standard Kubota L5030 experiment the sled was empty of weights. The velocity and engine speed targets for the reconfigured Kubota were the same as for the common Kubota configuration.

4.3 RESULTS

4.3.1 CLARK asphalt test on 30 November 2016

Data for CLARK were collected on the 30 November 2016. As this entire experiment was performed on asphalt, no soil samples were collected for a gravimetric water content calculation. Testing at W1, W2, W3, and W4 began at approximately 8:20 AM, 9:40 AM, 3:20 PM, and 4:00 PM eastern standard time. The atmospheric conditions are summarized by the mesonet data (Figure 4-19, and Figure 4-20).

Station ID	Relative Location	County	Location *to nearest hundreth	Observation Day	High Temp	Low Temp	Accum. Precip.	Sunrise/Sunset
LXGN	Lexington 7 S	Fayette	lat:37.98 lon:-84.53	Wed Nov 30 2016	60.7	56.5	0.02	7:38AM / 5:15PM

Time	Air Temperature (° F)	Relative Humidity (%)	Precipitation (in.)	Wind Speed (mph)	Wind Direction (°)	Wind Speed Max Gust (mph)	Solar Radiation (W/m^2)	Dewpoint (° F)
04:00 PM EST, 11/30/2016	58.3	79	0.00	12	W (259)	18	20	51.9
03:00 PM EST, 11/30/2016	59.7	78	0.00	13	SW (242)	17	95	53.0
02:00 PM EST, 11/30/2016	60.4	79	0.00	10	SW (223)	16	201	53.8
01:00 PM EST, 11/30/2016	59.4	83	0.00	9	SW (223)	12	136	54.2
12:00 PM EST, 11/30/2016	59.0	87	0.00	9	SW (232)	12	187	55.1
11:00 AM EST, 11/30/2016	58.8	91	0.00	10	SW (238)	13	115	56.0
10:00 AM EST, 11/30/2016	58.1	94	0.00	8	SW (234)	12	109	56.4
09:00 AM EST, 11/30/2016	58.3	93	0.00	9	SW (229)	12	25	56.4
08:00 AM EST, 11/30/2016	58.0	96	0.00	6	SW (204)	9	5	56.8
07:00 AM EST, 11/30/2016	56.8	98	0.00	6	S (191)	9	0	56.1
06:00 AM EST, 11/30/2016	56.8	98	0.00	4	S (178)	6	0	56.0
05:00 AM EST, 11/30/2016	57.1	98	0.00	5	SE (148)	8	0	56.4

Figure 4-19 Mesonet data for 30 November 2016

Monthly Climatological Summary *(11/2016)*

Station ID	LXGN
Relative Location	Lexington 7 S
County	Fayette County
Location *To Nearest Hundredth	Lat: 37.97°; Lon: -84.53°
Elevation	1044 ft.
Observation Day	Eastern Standard Time

Day	Date	Temperature (°F)				Degree Days		Humidity (%)		Precip (inch)	Wind Speed (mph) and Direction				Solar (MJ/ m²)
		Max	Min	Avg	Avg Dwpt	HDD	CDD	Max	Min		Res Dir	Res Spd.	Avg Spd.	Max 3-sec	
SUN	27	52	24.7	38.4	28.6	27	0	98	41	0	SSE	4.6	5.1	12.9	10.2
MON	28	59.2	45.2	52.2	40.3	13	0	97	47	0.46	SSE	9.7	10.5	37.3	2.5
TUE	29	63.4	46.3	54.8	47	10	0	96	50	0.09	SSW	7.2	8.2	29.8	10
WED	30	60.7	39.4	50	50.4	15	0	98	72	0.24	SW	6.3	8.1	31.3	3.6

Figure 4-20 Mesonet daily data before 30 November 2016

The following data were gathered for CLARK on asphalt (Table 4-5, Table 4-6, Table 4-7, and Table 4-8). It should be noted that the weight 4 (W4) data gathered using the small GPS receiver on the power analysis board were unreliable. The GPS coordinates recorded from the small GPS receiver on the power analysis board did not accurately reflect the path driven when the coordinates were flattened and plotted. The large Trimble MS990 did appear to accurately record the GPS data when flattened and plotted. Therefore, the Trimble GPS data were used only for CLARK weight 4. The GPS data for all other weights, including CLARK and the Kubota, appeared to be accurately recorded using the small GPS receiver on the power analysis board.

The current and voltage as recorded from the custom PCBs present a clear picture of the energy required for CLARK to pull the sled given the recorded conditions. The data files were processed to determine the average current and voltage for the given run. The current and voltage were recorded from CLARK's power analysis board. The force data were recorded from a second power analysis board instrumented to specifically record the force measurement. Both of these boards were recording the GPS data. The GPS time stamp on each file allowed the data to be synchronized between the files. Clearly seeing the force measurement begin and return to zero kilograms of force allowed the precise data points of the run to be extracted from the overall data.

Table 4-5 CLARK weight 1 run 1:3 on asphalt

		$F(N)_{ACTUAL}$	amp	volt	power (W)	dist.(m)	time(s)	vel.(m s^{-1})	E (kWh)
W1	R1	1163	80.16	79.12	6342.3	30.12	38	0.793	0.067
	R2	1215	83.04	78.91	6552.7	31.22	37	0.844	0.067
	R3	1141	85.17	78.65	6698.6	29.06	34	0.855	0.063
Avg.		**1173**	**82.79**	**78.89**	**6531.2**	***30.103***	***36.3***	***0.831***	***0.066***

Table 4-6 CLARK weight 2 run 1:3 on asphalt

		$F(N)_{ACTUAL}$	amp	volt	power (W)	dist.(m)	time(s)	vel.(m s^{-1})	E (kWh)
W2	R1	1532	98.94	78.16	7733.2	29.19	35	0.834	0.075
	R2	1451	97.25	78.10	7595.2	30.81	32	0.963	0.068
	R3	1573	100.42	77.82	7814.7	29.56	31	0.954	0.067
Avg.		**1519**	**98.87**	**78.03**	**7714.4**	***29.85***	***32.7***	***0.917***	***0.070***

Table 4-7 CLARK weight 3 run 1:3 on asphalt

		$F(N)_{ACTUAL}$	amp	volt	power (W)	dist.(m)	time(s)	vel.(m s^{-1})	E (kWh)
W3	R1	2542	129.9	78.58	10207.5	32.03	31	1.03	0.088
	R2	3260	142.0	77.88	11059.0	28.94	37	0.782	0.114
	R3	3167	146.4	77.50	11346.0	31.09	35	0.888	0.110
Avg.		**2990**	**139.4**	**77.99**	**10870.8**	***30.69***	***34.3***	***0.900***	***0.104***

Table 4-8 CLARK weight 4 run 1:3 on asphalt

		$F(N)_{ACTUAL}$	amp	volt	power (W)	dist.(m)	time(s)	vel.(m s^{-1})	E (kWh)
W4	R1	3883	168.1	76.67	12888.2	29.70	32	0.928	0.115
	R2	3811	167.5	76.33	12785.3	31.33	35	0.895	0.124
	R3	3726	171.4	75.99	13024.7	30.67	31	0.989	0.112
Avg.		**3807**	**169.0**	**76.33**	**12899.4**	***30.57***	***32.7***	***0.937***	***0.117***

4.3.2 Kubota L5030 asphalt test on 1 December, 2016

Data for Kubota L5030 common configuration were collected on 1 December 2016. Testing at W4, W3, W2, and W1 began at approximately 1:50 PM, 2:30 PM, 3:00 PM, and 3:20 PM eastern standard time. It is believed that the Kubota was at operating temperature throughout the experiment as the tractor was only turned off to take a reading from the flow meter once the experiment began. The atmospheric conditions are summarized by the mesonet data (Figure 4-21).

Monthly Climatological Summary *(12/2016)*

Station ID	LXGN
Relative Location	Lexington 7 S
County	Fayette County
Location *To Nearest Hundredth	Lat: 37.97°; Lon: -84.53°
Elevation	1044 ft.
Observation Day	Eastern Standard Time

Day	Date	Temperature (°F)				Degree Days		Humidity (%)		Precip (inch)	Wind Speed (mph) and Direction				Solar (MJ/ m²)
		Max	Min	Avg	Avg Dwpt	HDD	CDD	Max	Min		Res Dir	Res Spd.	Avg Spd.	Max 3-sec	
SAT	26	46.4	29.4	37.9	32	27	0	100	54	0	NE	2.8	3.4	11.9	6.7
SUN	27	53	26.3	39.7	30.6	25	0	100	34	0	ESE	1.8	3.1	10.2	8.3
MON	28	57.9	46.6	52.2	42.5	13	0	100	34	1.11	SSE	7.6	8.9	56.4	1.2
TUE	29	67.1	49.6	58.4	48.3	7	0	100	41	0.16	S	4.6	5.1	21.5	9.4
WED	30	58.1	40.1	49.1	42.8	16	0	100	56	0.22	W	4.4	5.2	19.2	4
THU	1	46.4	33.7	40.1	30.9	25	0	82	55	0	WSW	7.4	7.6	20.8	9.8

Figure 4-21 Mesonet daily data before 1 December 2016

The Kubota was used to pull the sled while the following data were collected. Weight 4 was recorded first, then weight 3, weight 2, and weight 1 as the concrete blocks were removed from the sled (Table 4-9, Table 4-10, Table 4-11, and Table 4-12).

Table 4-9 Common configuration Kubota weight 1 run 1:3 asphalt test

		$\overline{F(N)_{ACTUAL}}$	diesel used (L)	dist.(m)	time(s)	vel.(m s^{-1})	$\overline{E}$ (kWh)
W1	R1	1315	0.032	32.46	44	0.738	0.318
	R2	1503	0.032	30.85	43	0.717	0.318
	R3	1377	0.027	29.68	40	0.742	0.269
Avg.		**1398**	**0.030**	***31.00***	***42.3***	***0.732***	***0.302***

Table 4-10 Common configuration Kubota weight 2 run 1:3 asphalt test

		$\overline{F(N)_{ACTUAL}}$	diesel used (L)	dist.(m)	time(s)	vel.(m s^{-1})	$\overline{E}$ (kWh)
W2	R1	1944	0.031	29.28	44	0.665	0.308
	R2	2097	0.031	28.01	44	0.637	0.308
	R3	1972	0.026	31.93	41	0.780	0.259
Avg.		**2004**	**0.029**	***29.74***	***43***	***0.694***	***0.292***

Table 4-11 Common configuration Kubota weight 3 run 1:3 asphalt test

		$\overline{F(N)_{ACTUAL}}$	diesel used (L)	dist.(m)	time(s)	vel.(m s^{-1})	$\overline{E}$ (kWh)
W3	R1	2828	0.031	30.30	37	0.819	0.308
	R2	2659	0.026	30.63	36	0.851	0.259
	R3	2907	0.031	31.98	37	0.864	0.308
Avg.		**2798**	**0.029**	***30.97***	***36.7***	***0.845***	***0.292***

Table 4-12 Common configuration Kubota weight 4 run 1:3 asphalt test

		$\overline{F(N)_{ACTUAL}}$	diesel used (L)	dist.(m)	time(s)	vel.(m s^{-1})	$\overline{E}$ (kWh)
W4	R1	3555	0.052	32.69	37	0.884	0.517
	R2	3788	0.047	31.67	40	0.792	0.467
	R3	3689	0.031	31.62	37	0.855	0.308
Avg.		**3677**	**0.043**	***31.99***	***38***	***0.844***	***0.431***

4.3.3 Reconfigured Kubota L5030 asphalt test on 5 December 2016

Data for the reconfigured Kubota L5030 were collected on the 5 December 2016. Testing at W1, W2, W3, and W4 began at approximately 7:50 AM, 8:20 AM, 8:45 AM, and 9:00 AM eastern standard time. It is believed that the Kubota was at operating temperature throughout the experiment as the tractor was only turned off to take a reading from the flow meter once the experiment began. The atmospheric conditions are summarized by the mesonet data (Figure 4-22).

Monthly Climatological Summary *(12/2016)*

Station ID	LXGN
Relative Location	Lexington 7 S
County	Fayette County
Location *To Nearest Hundredth	Lat: 37.97°; Lon: -84.53°
Elevation	1044 ft.
Observation Day	Eastern Standard Time

Day	Date	Temperature (°F)				Degree Days		Humidity (%)		Precip (inch)	Wind Speed (mph) and Direction				Solar (MJ/ m^2)
		Max	Min	Avg	Avg Dwpt	HDD	CDD	Max	Min		Res Dir	Res Spd.	Avg Spd.	Max 3-sec	
SUN	27	52	24.7	38.4	28.6	27	0	98	41	0	SSE	4.6	5.1	12.9	10.2
MON	28	59.2	45.2	52.2	40.3	13	0	97	47	0.46	SSE	9.7	10.5	37.3	2.5
TUE	29	63.4	46.3	54.8	47	10	0	96	50	0.09	SSW	7.2	8.2	29.8	10
WED	30	60.7	39.4	50	50.4	15	0	98	72	0.24	SW	6.3	8.1	31.3	3.6
THU	1	46.4	33.7	40.1	30.9	25	0	82	55	0	WSW	7.4	7.6	20.8	9.8
FRI	2	44.2	29.8	37	29.3	28	0	90	60	0	WNW	3.8	5	15.6	8.9
SAT	3	40.8	37.3	39	30.6	26	0	81	64	0	NNE	2	3.2	10.5	3.6
SUN	4	45.3	36.6	41	36.7	24	0	97	72	0.08	SE	3.8	6.9	19.6	3.4
MON	5	44.1	38.5	41.3	36.9	24	0	94	73	0	ENE	2.5	6.8	19.8	4.3

Figure 4-22 Mesonet daily data before 5 December 2016

The Kubota was used to pull the sled while the following data were collected (Table 4-13, Table 4-14, Table 4-15, and Table 4-16). When the end of the run was reached the tractor was backed up enough for the force on the load cell to drop to zero kilograms then turned off for a reading from the Fuel View flow meter. As has been mentioned, the tractor was turned off before the run began, and at the end. Weight 1 was recorded first, then weight 2, weight 3, and weight 4 as the concrete blocks were added to the sled.

Table 4-13 Custom configuration Kubota weight 1 run 1:3 asphalt test

		$\overline{F(N)_{ACTUAL}}$	diesel used (L)	dist.(m)	time(s)	vel.(m s^{-1})	$\overline{E}$ (kWh)
W1	R1	1274	0.057	28.64	51	0.562	0.567
	R2	1361	0.062	29.16	51	0.572	0.617
	R3	1301	0.057	30.40	51	0.596	0.567
Avg.		**1312**	**0.059**	***29.40***	***51***	***0.577***	***0.584***

Table 4-14 Custom configuration Kubota weight 2 run 1:3 asphalt test

		$\overline{F(N)_{ACTUAL}}$	diesel used (L)	dist.(m)	time(s)	vel.(m s^{-1})	$\overline{E}$ (kWh)
W2	R1	1873	0.060	32.75	53	0.618	0.567
	R2	1807	0.051	28.80	51	0.565	0.507
	R3	2176	0.052	29.27	53	0.552	0.517
Avg.		**1952**	**0.054**	***30.27***	***52.3***	***0.578***	***0.540***

Table 4-15 Custom configuration Kubota weight 3 run 1:3 asphalt test

		$\overline{F(N)_{ACTUAL}}$	diesel used (L)	dist.(m)	time(s)	vel.(m s^{-1})	$\overline{E}$ (kWh)
W3	R1	2416	0.051	33.12	46	0.720	0.507
	R2	2753	0.046	29.86	44	0.679	0.457
	R3	2693	0.047	29.61	44	0.673	0.467
Avg.		**2621**	**0.048**	***30.86***	***44.7***	***0.691***	***0.477***

Table 4-16 Custom configuration Kubota weight 4 run 1:3 asphalt test

		$\overline{F(N)_{ACTUAL}}$	diesel used (L)	dist.(m)	time(s)	vel.(m s^{-1})	$\overline{E}$ (kWh)
W4	R1	3471	0.051	32.34	43	0.752	0.507
	R2	3108	0.046	31.88	44	0.725	0.457
	R3	3268	0.051	31.84	43	0.741	0.507
Avg.		**3282**	**0.049**	***32.02***	***43.3***	***0.739***	***0.490***

4.3.4 Data summary

Data from CLARK can be summarized according to the power and energy data (Table 4-17).

Table 4-17 CLARK data summary

	CLARK		
	$\overline{F(N)_{ACTUAL}}$	$\overline{Power\ (W)}$	$\overline{E(kWh)}$
W1	1173	6531.2	0.066
W2	1519	7714.4	0.070
W3	2990	10870.8	0.104
W4	3807	12899.4	0.117

The Kubota data can also be summarized according to energy (Table 4-18).

Table 4-18 Kubota data summary

	Kubota L5030					
	common configuration			custom configuration		
	$\overline{F(N)_{ACTUAL}}$	diesel used (L)	$\overline{E(kWh)}$	$\overline{F(N)_{ACTUAL}}$	diesel used (L)	$\overline{E(kWh)}$
W1	1398	0.030	0.302	1312	0.059	0.584
W2	2004	0.029	0.292	1952	0.054	0.540
W3	2798	0.029	0.292	2621	0.048	0.477
W4	3677	0.043	0.431	3282	0.049	0.490

4.4 DISCUSSIONS

4.4.1 Load cell verification

Upon completion of the experiment, the power analysis board, load cell, and the instrumentation amplifier were set up and tested with the hydraulic press as a verification. This provided an accurate verification for the entire force measurement system ensuring the data were valid throughout the experiment. The hydraulic press was turned on and the Fluke 700G was zeroed at 0 kPa. Then the pressure was increased to 827, 2054, 3426, 4481, 5171, 5860, 6922, 7577, 8273, and 8963 kPa which generated forces of 3242, 8051, 13429, 17561, 20266, 22966, 27129, 29696, 32423, and 35127 N as measured by the Fluke 700G to verify over the entire range of forces as was done during the calibration (Table 4-19). The measured force was read from the Arduino Mega on the serial monitor while the actual force was calculated from the Fluke 700G measured pressure (Equation 4-7).

Table 4-19 Load cell verification data

P(kPa)	$F(N)_{ACTUAL}$ From Eq. 5-3	$\lvert F(N)_{RECORDED} \rvert$ Arduino logged
827	3242	3767
2054	8051	9710
3426	13429	15511
4481	17561	20146
5171	20266	22899
5860	22966	25942
6922	27129	30723
7577	29696	33477
8273	32423	36377
8963	35127	39566

These data were plotted and trend lines were calculated (Figure 4-23). This process verified the load cell data were reliable throughout the experiment.

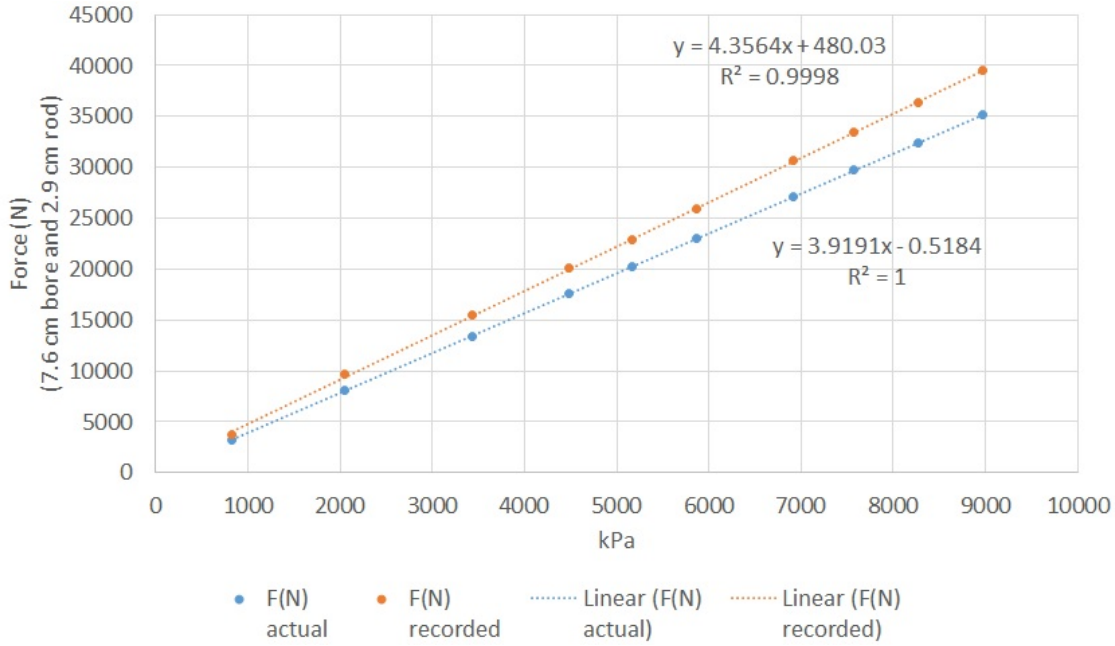

Figure 4-23 Load cell verification on 15 December 2016

The correlation coefficient for the verification curve and the calibration curve both indicate a good linear fit for the load cell response. The y-intercept of the recorded verification curve was approximately 157 N lower than the y-intercept of the recorded calibration curve. There is also a small difference in slope between the two curves.

4.4.2 CLARK and Force vs Current model

It is apparent that the CLARK instrumentation was very capable to capture any increase in consumed current or droop in voltage. A change in consumed current was measured for each change in weight. As such, a nice correlation between drawbar force and consumed current can be modeled. For this plot, the recorded force (Table 4-5, Table 4-6, Table 4-7, and Table 4-8) was corrected by the calibration curve so that the actual force could be plotted. From the calibration curve, the following formula (Equation 4-8, Equation 4-9, and Equation 4-10) were used to correct the recorded force yielding the actual force (Table 4-20).

Table 4-20 CLARK Force vs Current relationship

CLARK	_____ (amp)	_____ $F(N)_{RECORDED}$	_____ $F(N)_{ACTUAL}$
W1	82.79	1912	1173
W2	98.87	2288	1519
W3	139.4	3888	2990
W4	169.0	4776	3807

Now, it is straightforward to plot the actual force (N) versus the consumed current (amp) to see the relationship (Figure 4-24).

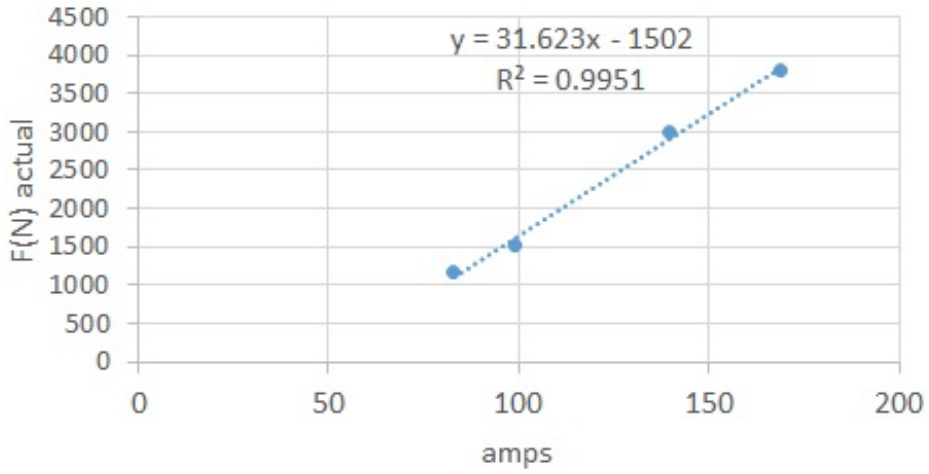

Figure 4-24 CLARK Force vs. Current

From the above plot, it is possible to model the draw bar force ($F_{DRAWBAR}$) from a current (amp) measurement (Equation 4-11).

$$F_{DRAWBAR} = 31.623 * Current - 1502 \qquad \text{Equation 4-11}$$

4.4.3 Kubota – common configuration

The total distance driven was comparable, as only 2.25 m separated the longest average distance from the shortest average distance. However, the recorded consumed fuel did not capture the difference in weights on the sled. W1, W2, and W3 all recorded very

similar energy requirements (being approximately 0.292 kWh). W4 run 3 (W4R3) also reported a similar energy requirement (0.308 kWh) while W4R1 and W4R2 reported a higher energy requirement (close to 0.50 kWh). What can be said, is that at W1, W2, W3, and W4 CLARK respectively consumed 22%, 24%, 36%, and 27% of the required energy as compared to the Kubota common configuration.

It is possible that subtle differences by the operator or total time at a given engine speed overshadow the difference in weight on the sled as seen by the Kubota. This could possibly explain why W4R1 and W4R2 were higher than W4R3. If this is the case, then a much longer test course with more runs may capture the difference in consumed energy at each weight point.

4.4.4 Kubota – custom configuration

The total distance driven was comparable, as only 2.6 m separated the longest average distance from the shortest average distance. However, the recorded consumed fuel did not capture the difference in weights on the sled. W1, W2, W3, and W4 all recorded very similar energy requirements (close to 0.50 kWh). What can be said, is that at W1, W2, W3, and W4 CLARK respectively consumed 11%, 13%, 22%, and 24% of the required energy as compared to the Kubota custom configuration. As the Samson 9.5-24 rear tires used in this reconfigured Kubota are smaller than the stock 14.9-26 tires on the Kubota, the time to finish a run increased for the reconfigured Kubota as compared to the common Kubota configuration.

The Kubota common and custom configuration tire inflation pressure was not matched to the tire inflation pressure of CLARK. This is consistent as the front tires on CLARK were different than the front tires on the Kubota. The different front tire size, tread, and inflation pressure each contribute a subtle difference to the rolling resistance of the vehicle.

4.5 CONCLUSIONS

Power, energy, and draft force data were collected over a range suitable for a category 1 tractor. Data were collected for a fully electric tractor alongside data for a Kubota L5030 in a common and custom configuration matching the weight distribution of

the electric tractor that could be used for comparison purposes. These data were used to create a model relating the drawbar force with the required current drawn from a battery of a fully electric tractor.

CLARK did consume less than half of the energy compared to the Kubota L5030 at four distinct weight points utilizing a weighted sled and a drawbar attachment. CLARK consumed 22%, 24%, 36%, and 27% of the energy as compared to the Kubota L5030 common configuration for the weight points W1, W2, W3, and W4 respectively. CLARK consumed 11%, 13%, 22%, and 24% of the energy as compared to the Kubota L5030 custom configuration for the weight points W1, W2, W3, and W4 respectively.

- The average power and energy requirement for CLARK corresponding to the four weight points was determined and is summarized in (Table 4-17) and repeated here.

	CLARK		
	$\overline{F(N)_{ACTUAL}}$	Power (W)	E(kWh)
W1	1173	6531.2	0.066
W2	1519	7714.4	0.070
W3	2990	10870.8	0.104
W4	3807	12899.4	0.117

- The following correlation between required drawbar force ($F_{DRAWBAR}$) and the current drawn out of the battery (A) for the weight point data was determined in (Equation 4-11) and is repeated here.

$$F_{DRAWBAR} = 31.623 * Current - 1502$$

- The average fuel consumed by the Kubota L5030 in each configuration to pull the weighted sled at the four weight points was determined and is summarized in (Table 4-18) and repeated here.

	Kubota L5030					
	common configuration			custom configuration		
	$\overline{F(N)_{ACTUAL}}$	diesel used (L)	$\overline{E(kWh)}$	$\overline{F(N)_{ACTUAL}}$	diesel used (L)	$\overline{E(kWh)}$
W1	1398	0.030	0.302	1312	0.059	0.584
W2	2004	0.029	0.292	1952	0.054	0.540
W3	2798	0.029	0.292	2621	0.048	0.477
W4	3677	0.043	0.431	3282	0.049	0.490

CHAPTER 5: 15 KW PHOTOVOLTAIC ARRAY POWER SOURCE

5.1 INTRODUCTION

In 1987 the Brundtland Commission defined sustainability as "meeting the needs of the present without compromising the ability of future generations to meet their own needs" (World Commission on Environment and Development, 1987). Given the above definition, solar energy is a sustainable source of energy whereas fossil fuels are not sustainable sources. The US Department of Energy estimates the total world energy demand is approximately 500 quadrillion (500E15) BTU per year (US Energy Information Administration, 2013). Furthermore, solar possibilities could easily meet these energy needs (US Department of Energy, Solar FAQs, 2006). This all builds a very compelling case for solar as a viable alternative energy source to the more conventional fossil fuel sources. However, the requirements for replacing a conventional fossil fuel tractor with a solar sourced battery powered electric tractor are not well understood at this time. Liquid combustible fossil fuels have a high energy to mass and energy to volume ratios compared to electrical energy storage methods. This provides simplicity in system design as energy storage is not a huge design factor in developing systems that rely on fossil fuels. If one converts a tractor's energy storage to batteries, what effect does this have on the system design? How many tasks could this battery powered electric tractor assume from a traditional fossil fuel tractor? What size of solar electric power system would maximize the usefulness of the battery powered electric tractor and minimize the greenhouse gases? There are a variety of agricultural production systems with considerable diversity in machinery and energy usage patterns. The focus of this experiment will be on machinery and energy usage patterns of a diversified organic vegetable production CSA farm, as these production systems would be able to leverage solar energy usage in marketing and pricing decisions.

The University of Kentucky currently operates a 12 acre diversified organic vegetable production CSA farm. While this farm is an active CSA and must cover its expenses with customer purchases, its status as a research farm provides detailed records of machinery and energy use. As such, this CSA provides an ideal environment to

understand the energy requirements for this type of vegetable production farming. After considering the various machinery tasks on the CSA farm, weed control operations appeared to be the most suitable task for initial conversion to a battery powered tractor. These weed control operations most closely matched the definition of utility-type tasks (R. Alcock, 1983) being frequently used throughout the summer, but only for short durations at any one time. The primary weed control implement on the UK CSA was a finger weeder (Figure 5-1). This implement was suitable for a 20 HP tractor with a category 1 three-point hitch.

The University of Kentucky CSA also utilized significant electrical energy for product processing and storage. All of the electrical energy used on the CSA was provided by a single electric meter dedicated to the CSA. This experiment also considered the requirement of this conventional electric energy use in determining the size of an on-site renewable energy generation system based on a photovoltaic (PV) array. The PV array should be sized to supply the energy for CLARK to finger weed and still meet the UK CSA conventional electric needs. The hypothesis for this experiment is based on a 15 kW solar PV system that will be used later in this chapter. A model was developed relating drawbar force, battery size, and the working time at the given force. Another model was developed to balance the conventional electric energy needs of a CSA farm and the estimated energy needs of a fully electric tractor with the net electric energy produced from a PV array.

5.2 Material and Methods

The custom built electric tractor used for this experiment has already been detailed in chapter 4 (Figure 4-1). The Kubota L5030 used to collect the conventional diesel usage has also been described in chapter 4 (Figure 4-6). No further modifications to CLARK or the L5030 were required for this experiment.

A K.U.L.T.-Kress finger weeder (Figure 5-1) was chosen as the implement to use for this experiment. The tool is designed to be driven along a bed and weed the two rows of produce within the bed. The rubberized fingers turn in between the crop row to dislodge small weeds around the crop. In addition, the sweeps disturb the soil at a small distance from the crop to disrupt any unwanted growth, yet not affecting the crop plant itself. The

depth and width of the sweeps and fingers can be adjusted at the operator's discretion. The cultivator can be steered independently of the tractor to allow for precision cultivation.

Figure 5-1 K.U.L.T.-Kress finger weeder

The mesonet data station mentioned in chapter 4 is located on the UK CSA. In addition to the mesonet data, four soil core samples were taken from various locations within the crop bed and four from various locations within the more compacted ground that was driven on by the tractors. These samples were placed in an airtight plastic cup for weighing and drying. A total weight was recorded including the cup, lid, and wet soil. The cup containing the wet sample was then dried for 24 hours at 104°C alongside the lid for tracking purposes. The dried sample was then weighed again to obtain a dry mass. From these measurements the soil gravimetric water content (u) can be calculated (Equation 5-1).

$$u = \frac{MASS_{WET\_SAMPLE} - MASS_{DRY\_SAMPLE}}{MASS_{DRY\_SAMPLE}} = \frac{MASS_{WATER}}{MASS_{SOIL}} \qquad \text{Equation 5-1}$$

5.2.1 CSA finger weeding frequency in 2015

The CSA tracks many metrics throughout the growing season. For instance, the finger weeding data recorded in 2015 included the day, duration, total number of beds, number of hours to complete the task, the tractor used, the specific crop, field number, and number of staff required. These data were compiled and used to calculate an annual energy estimate to finger weed.

5.2.2 CSA conventional electricity usage in 2015

The CSA has a single electric meter (Figure 5-2) measuring all of the conventional electric needs of the CSA. The electric bills for this meter were collected and compiled for 2015.

Figure 5-2 CSA conventional electric meter

The single largest electricity user on this meter is a large walk-in cooler (Imperial Brown Inc., Salisbury, North Carolina, USA) used to store the vegetables. The cooler (Figure 5-3) measured (Height x Width x Depth) 2.6 x 5.3 x 4.7 meters. Other electricity users utilized by the CSA include a barrel washer (A.Z.S. Brusher Equip. LLC, Ephrata, Pennsylvania, USA), brush washer (A.Z.S. Brusher Equip. LLC, Ephrata, Pennsylvania, USA), and a Greens Machine spin dryer (Electrolux Professional, Inc., Charlotte, North Carolina, USA).

Figure 5-3 CSA walk in cooler

5.2.3 CLARK finger weeding

The weight of each tractor was recorded using a wheel scale (Figure 4-9). A scale was placed in front of a tire and the tractor was driven onto the scale for measurement. The scales used utilized a Vernier measurement allowing precision to the tens of kilograms. The inflation pressure of each tire was also recorded for thoroughness (Table 5-1). Fertilizer weighing 45 kg were added to the front of CLARK and 90.7 kg of fertilizer were added to the rear of CLARK as ballast for this experiment.

Table 5-1 CLARK to finger weed in the field weight distribution

CLARK in the field				
	Left wheel		Right wheel	
	kg	kPa	kg	kPa
Front	372	310	372	310
Rear	735	207	726	207

A plot was chosen and rows were identified to finger weed. While CLARK performed the task, GPS data were recorded via the onboard custom PCBs designed for the tractor. This allowed for a precise start time, stop time, and distance traveled. In addition, the current and voltage used during the task were recorded. Thus, the total power used was readily available from the collected data. Data were collected from finger weeding two beds in the same plot that the Kubota had previously worked. CLARK was aligned on the first bed for data collection (recorded as bed9 in this experiment) and then the finger weeder was lowered onto the ground and the tractor was turned off. The data file was erased before the experiment began so as to reduce unnecessary entries in the data file. The operator would climb aboard the finger weeder and indicate the task could begin. After the task was completed at the end of the row CLARK would stop and be turned off. This allowed a clear stopping point in the data file and allowed the operator to dismount from the finger weeder. The finger weeder would then be raised and CLARK was repositioned on the next bed for data collection (recorded as bed1 in this experiment). CLARK was turned off so the operator could mount the finger weeder and indicate the task could begin. CLARK was then turned on and proceeded to finger weed once a GPS lock was established. At the end of bed1 the tractor was again turned off.

5.2.4 Kubota reconfigured with 9.5-24 Samson tires to finger weed

From the same plot additional rows were identified for the Kubota to finger weed. The Kubota was configured with wheel centers to allow the same rear tires CLARK used. The Kubota was also ballasted to match the distribution of CLARK. Each rear tire had approximately 204 kg of ballast added to the custom wheel centers. Two suitcase weights were present for a total of 50 kg of additional ballast on the front of the L5030. In addition, 136 kg of fertilizer was added to the Kubota to match the CLARK weight distribution. The

weights recorded (Table 5-2) include the weight of the driver. The Kubota was driven at approximately 0.8 m s^{-1} using an engine speed of approximately 1700 RPM. The rows in the field were approximately 91 m in length. However, this experiment did not run the finger weeder to the very end of each row. The tractor was stopped short so as not to interfere with the drip tape and to remain in the flat portion of the plot before beginning to climb onto the greenway.

Table 5-2 Reconfigured Kubota to finger weed weight distribution

Kubota with 9.5-24 Samson rear rims in the field				
	Left wheel		Right wheel	
	kg	kPa	kg	kPa
Front	372	207	372	207
Rear	717	207	735	207

The Kubota would align on a row and then lower the finger weeder. The Kubota was turned off and the fuel meters that were installed on the injection and return lines were read. When the operator on the finger weeder indicated that the task could begin the Kubota would be turned on. At the end of the row, the fuel meters would be read immediately upon stopping and turning off the engine. This allowed for the consumed fuel to be accurately measured alongside the known velocity from the speedometer on the Kubota and the known distance of the row.

5.3 RESULTS

5.3.1 CLARK finger weeding on 26 October 2016

Data for CLARK were collected on 26 October 2016. The atmospheric conditions are summarized by the mesonet data (Figure 5-4).

Monthly Climatological Summary *(10/2016)*

Station ID	LXGN
Relative Location	Lexington 7 S
County	Fayette County
Location *To Nearest Hundredth	Lat: 37.97°; Lon: -84.53°
Elevation	1044 ft.
Observation Day	Eastern Standard Time

Day	Date	Temperature (°F)				Degree Days		Humidity (%)		Precip (inch)	Wind Speed (mph) and Direction				Solar (MJ/ m^2)
		Max	Min	Avg	Avg Dwpt	HDD	CDD	Max	Min		Res Dir	Res Spd.	Avg Spd.	Max 3-sec	
FRI	21	54.7	46.5	50.6	46.4	14	0	97	66	0.13	NW	10	10.1	24	6.2
SAT	22	56.6	41.8	49.2	38.1	16	0	93	46	0	WNW	5.3	6	18.6	15.4
SUN	23	70.6	41.3	55.9	42.8	9	0	83	43	0	SW	8.7	9	24.1	15.5
MON	24	66.1	50.1	58.1	44.5	7	0	78	41	0	NW	3.9	7.2	17	15.5
TUE	25	63.5	42.5	53	38.5	12	0	86	34	0	E	5.6	5.9	15	13.9
WED	26	76.1	44.1	60.1	44.3	5	0	77	39	0	SSE	4.8	7.7	23.2	13.8

Figure 5-4 Mesonet data from 26 October 2016

In addition, soil samples were taken throughout the field to characterize the gravimetric moisture content of the field as was done for the Kubota. Samples were taken in bed1 (b1), bed4 (b4), bed6 (b6), and bed7 (b7). Samples were also taken in four compacted tire track areas throughout the field at track2 (t2), track5 (t5), track7 (t7), and track8 (t8). As this field was still irrigated, moisture content was expected to be similar throughout the field. It was found that on this day the gravimetric moisture content was similar for the beds and the compacted tire track area throughout the field (Table 5-3). The conditions in the field were comparable to the conditions that existed when the data from the Kubota were taken on 19 October 2016.

Table 5-3 Soil data from 26 October 2016

	soil(g)	water(g)	*u* (as %)
b1	29.19	5.35	18.33%
b4	32.51	6.12	18.82%
b6	34.34	6.93	20.18%
b7	33.17	6.81	20.53%
average			19.47%
t2	41.45	7.90	19.06%
t5	48.28	9.19	19.03%
t7	40.85	7.92	19.39%
t8	42.38	8.41	19.84%
average			19.33%

The current (Figure 5-5, Figure 5-7) and voltage (Figure 5-6, Figure 5-8) as recorded from the custom PCBs present a clear picture of the energy required for CLARK to finger weed given the recorded conditions. Seeing the actual plot of the data allows for the spatial and temporal variability of the field work to be seen. For instance, the ground could be somewhat harder in a location or possibly sloped in one location and not another.

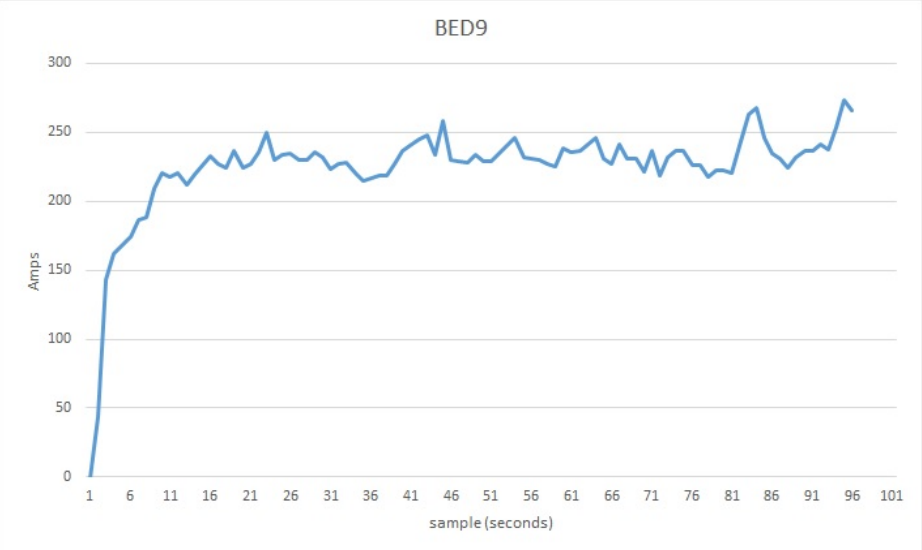

Figure 5-5 CLARK current for bed9

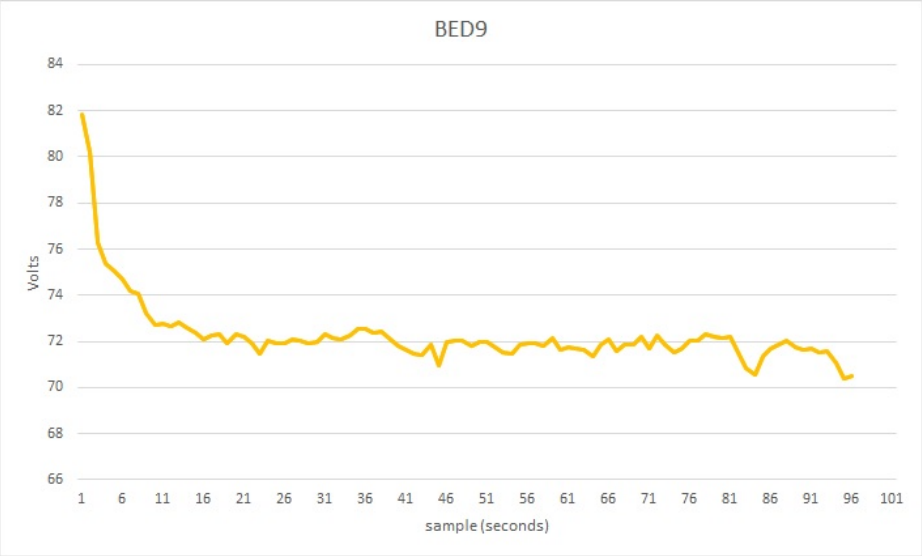

Figure 5-6 CLARK voltage for bed9

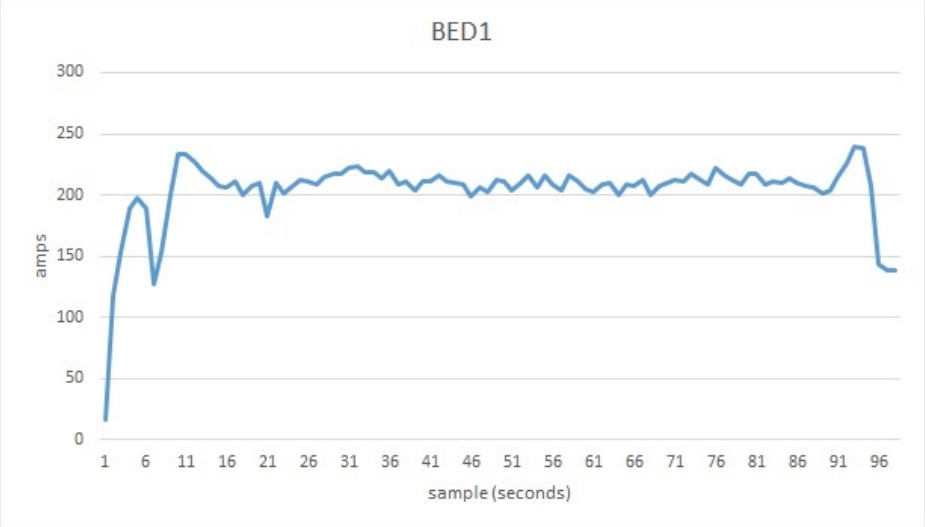

Figure 5-7 CLARK current for bed1

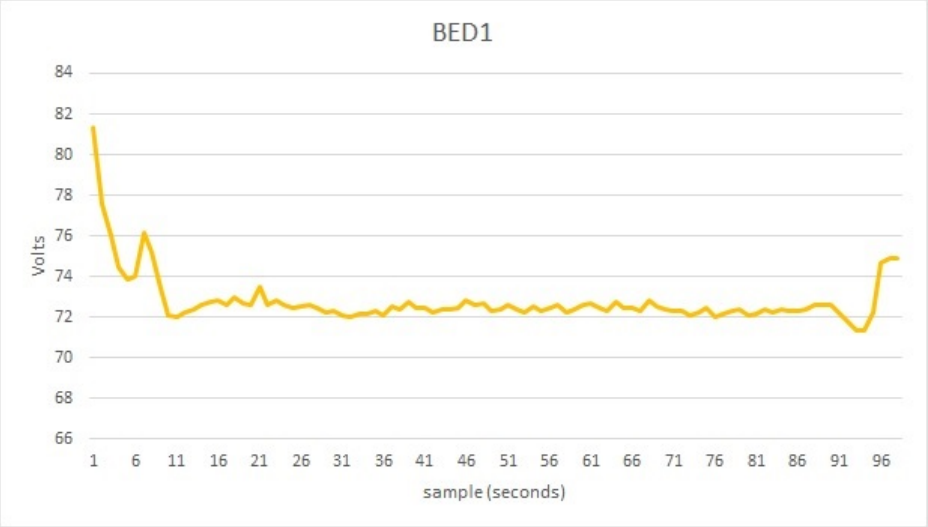

Figure 5-8 CLARK voltage for bed1

The distance can be accurately calculated from the processed GPS file. Since the time stamp is also recorded from the GPS file, a precise working time can also be calculated. All of the data from CLARK are summarized in (Table 5-4). The average current load for finger weeding was 214 amps. As this average load increases, the battery begins to droop and the capacity diminishes for the increased load. It was estimated that the Kress finger weeder required a drawbar pull of approximately 5,265 N (Equation 4-11).

Table 5-4 CLARK finger weeding summary

	average current (amp)	average volts (V)	average power (W)	time (s)	average energy (kWh)	distance (m)	velocity (m s^{-1})
bed9	224.34	72.28	16153.4	88	0.395	71.09	0.808
bed1	203.8	72.78	14832.6	104	0.428	77.05	0.741
average	**214.07**	72.53	15496	96	**0.412**	74.07	0.7745

5.3.2 Kubota reconfigured to finger weed on 19 October 2016

Data for the Kubota L5030 reconfigured to match CLARK were collected on 19 October 2016. The atmospheric conditions are summarized by the mesonet data (Figure 5-9).

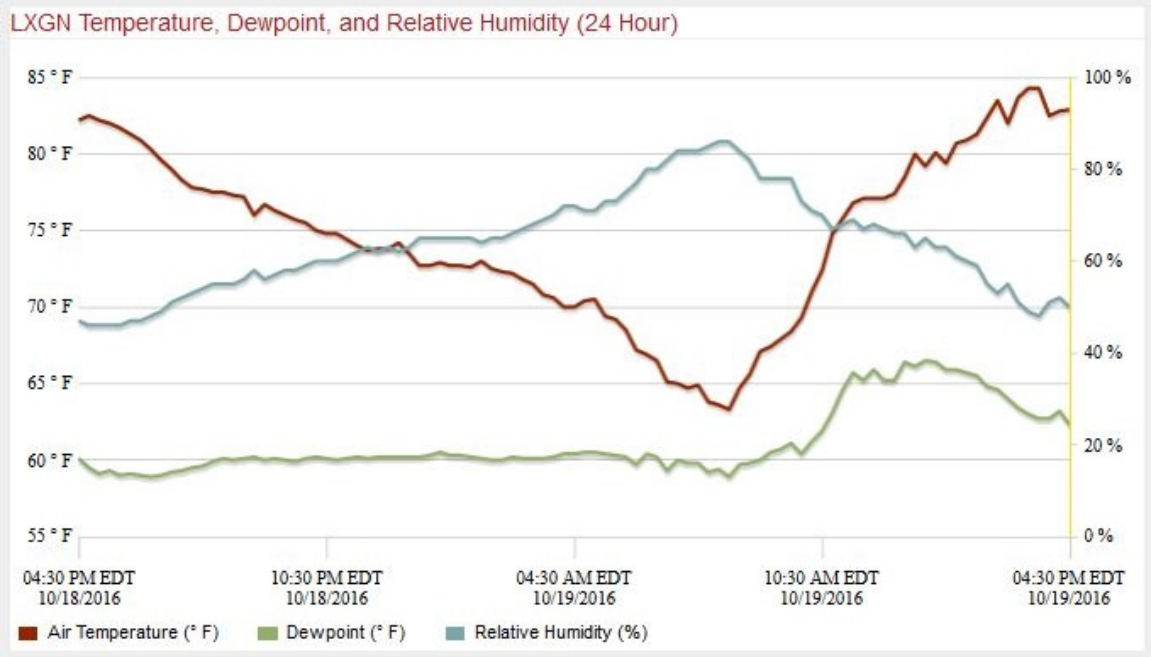

Station	Fayette County, KY
Time	10/19/2016, 04:30 PM EDT
Air Temperature	82.9 ° F
Relative Humidity	50 %
Precipitation	0.00 in.
Wind Speed	7 mph
Wind Direction	241 ° (SW)
Wind Speed Max Gust	10 mph
Solar Radiation	484 W/m^2
Dewpoint	62.3 ° F

Figure 5-9 Mesonet data from 19 October 2016

In addition, soil samples were taken throughout the field to characterize the gravimetric moisture content of the field. Samples were taken in bed1 (b1), bed4 (b4), bed6 (b6), and bed7 (b7) to be consistent with previous sampling. Samples were also taken in four compacted tire track areas throughout the field at track2 (t2), track5 (t5), track7 (t7), and track8 (t8). This field was irrigated, so moisture content was expected to be similar throughout the field. It was found that on this day the gravimetric moisture content was similar for the beds and the compacted tire track area throughout the field (Table 5-5).

Table 5-5 Soil data from 19 October 2016

	soil(g)	water(g)	*u (as %)*
b1	28.23	4.70	16.65%
b4	28.41	4.86	17.11%
b6	28.90	6.52	22.56%
b7	27.56	5.44	19.74%
average			19.01%
t2	45.52	8.10	17.79%
t5	44.27	8.00	18.07%
t7	39.91	7.73	19.37%
t8	39.34	6.78	17.23%
average			18.12%

The Kubota was used to finger weed bed1 and bed7 in the plot while the following data were collected (Table 5-6). A diesel fuel energy density of 35.8 MJ L^{-1} was used for this calculation.

Table 5-6 Kubota reconfigured to finger weed

	rpm	m s^{-1}	liters	kWh
b1	1700	0.805	0.145	1.442
b7	1700	0.805	0.108	1.074
average			0.1265	**1.258**

5.3.3 CSA finger weeding frequency in 2015

Finger weeding data as recorded by the CSA crew were processed to determine the frequency and duration of this task (Figure 5-10). From the data, it can be seen that a weekly maximum for the CSA was approximately 4 hours of finger weeding occurring the week of 9 to 15 August. As a note, 3.52 hours of work were performed on 9 August with 0.5 hours of finger weeding occurring on 15 August for this week. It should also be noted that 1.24 hours of finger weeding were performed on 15 September with 0.5 hours of work being done on 16 September. It can be seen that a daily maximum for the CSA was

approximately 3.5 hours of finger weeding occurring on 12 June and the 3.52 hours on 9 August. The monthly maximum was June with 5.5 hours of finger weeding. The annual total was 17.6 hours of finger weeding in 2015.

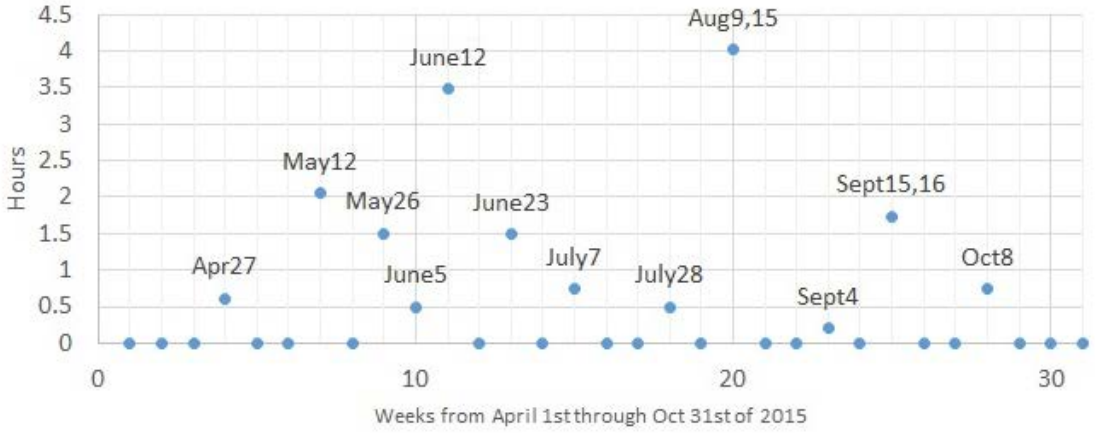

Figure 5-10 Finger weeding by hours each week (actual date recorded on data label).

This same data could also be presented as the number of beds where finger weeding occurred each week (Figure 5-11). On 9 August finger weeding was performed on two beds while on 15 August work was done on twenty-two beds. On 15 September finger weeding was performed on twelve beds while on 16 September only one bed was worked.

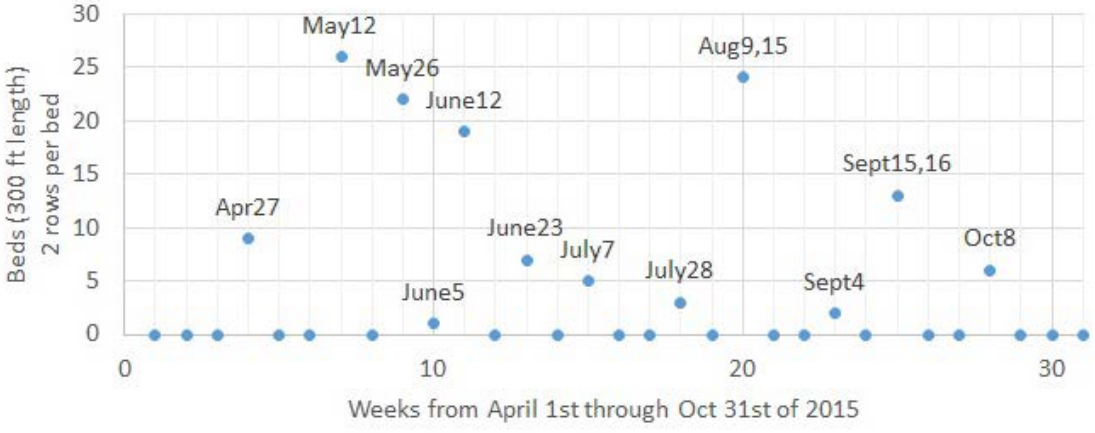

Figure 5-11 Finger weeding by beds each week (actual date recorded on data label).

It is also worth noting that the daily bed maximum occurred on 12 May with a total of twenty-six beds. The monthly bed maximum was May with a total of 48 beds. For the year of 2015, finger weeding of a 91 m bed was performed a total of 137 times.

5.3.4 CSA conventional electricity usage in 2015

The electric energy usage data were collected from the CSA (Table 5-7). For clarity, only the CSA electric needs are measured by this electric meter. A plot of this data is presented (Figure 5-12).

Table 5-7 CSA conventional electric usage for 2015

Billed on	(kWh)
15 Jan. 2015	749
12 Feb. 2015	624
17 Mar. 2015	692
16 Apr. 2015	658
15May2015	781
16 June 2015	997
16 July 2015	1455
17 Aug. 2015	1975
17 Sept. 2015	1571
16 Oct. 2015	1820
13 Nov. 2015	1319
14 Dec. 2015	961
Avg.	1134

Figure 5-12 CSA conventional electric usage for 2015

5.3.5 NREL solar data for Kentucky

The National Renewable Energy Laboratory (NREL) has recorded solar photovoltaic resource potential for the United States including this data for central Kentucky (Table 5-8, Figure 5-13). This data are presented as monthly averages from 1998 to 2008. These maps represent average photovoltaic solar resource available using a grid size of approximately 10 km (NREL, 2016). As can be seen, NREL estimates that over the year a daily average of 4.5 kWh m^{-2} day^{-1} can be expected. A peak sun hour is an hour in which the intensity of sunlight is 1 kW m^{-2} (How to Calculate your Peak Sun-Hours, 2016). Therefore, an average solar resource of 4.5 kWh m^{-2} day^{-1} is commonly referred to as 4.5 peak sun hours per day (Average Solar Radiation, 2017). Central Kentucky is historically expected to have an average of 4.5 peak sun hours each day to produce electricity.

Table 5-8 NREL solar photovoltaic resource potential for Kentucky

1998-2008	(kWh m^{-2} day^{-1})
Jan	3.25
Feb	4.25
Mar	4.75
Apr	4.75
May	5.25
Jun	5.25
July	5.25
Aug	5.25
Sept	5.25
Oct	4.25
Nov	3.25
Dec	2.75
Avg.	4.5

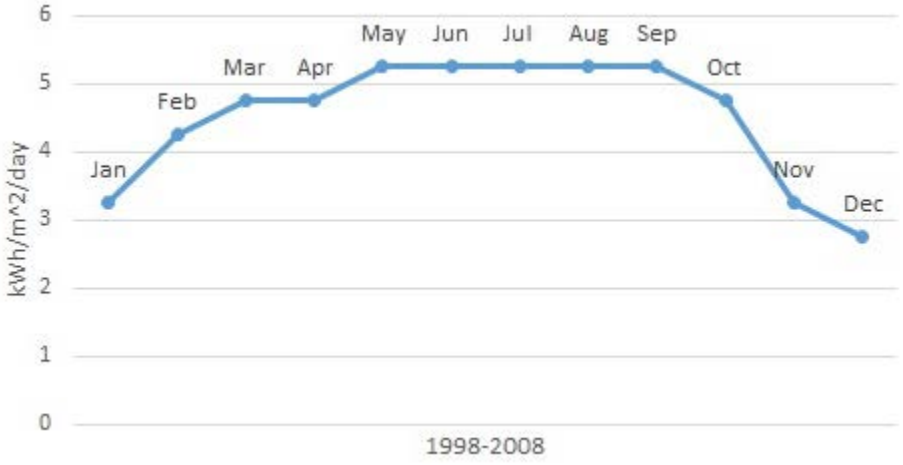

Figure 5-13 NREL solar photovoltaic resource potential for KY

5.4 DISCUSSIONS

5.4.1 Energy and capacity

The weather conditions and the gravimetric moisture content of the field were similar for 19 October and 26 October. The reconfigured Kubota matched CLARK in weight distribution and the same Samson 9.5-24 rear tires were used for both tractors.

Considerable effort was used to make the field comparison meaningful between these two very different tractors performing the same task in the same field.

The Kubota consumed approximately 1.258 kWh of energy while CLARK consumed approximately 0.411 kWh of energy to finger weed each bed. The ZAPI inverters do not list the efficiency, however high efficiency inverters are commonly rated at 90-95% efficiency. In addition, CLARK did not have a transmission to incur any further mechanical loses. With these known characteristics, CLARK was expected to be more energy efficient given the same task under similar conditions.

The distance recorded from bed9 was shorter than the distance from bed1. When looking at the current and voltage plots of the data from bed9 it is also apparent that the data ends abruptly. The data from bed1 ends in a more predictable manner. Meaning, the current drops off to zero amps and the voltage recovers once the load of finger weeding is removed from the battery for bed1. This is all consistent with the fact that CLARK had an unexpected shut down towards the very end of bed9. It is believed that the power draw was significant enough that the control electronics in the ZAPI controller issued a shut down and restart. It was decided at that time to simply take the data we had for that row and consider it as being a few meters short.

The real question now becomes, can the battery on CLARK store and deliver enough energy to be useful for the CSA? As has been stated, the battery used in this experiment was a 40-125-7 lead-acid battery from Crown (375 Ah and 80 V). It was measured in the field that CLARK needs on average 214 amps to finger weed. Derating information was provided by Crown and allowed for a mathematical model to be developed. For clarification, the information (Table 5-9) says that given a 6 hour discharge window, 375 Ah of capacity are available. Given a 1 hour discharge window, 202.5 Ah of capacity are available.

Table 5-9 Crown 40-125-7 derating information provided by Crown

discharge window (hours)	capacity% (decimal)	capacity (Ah)	amp
6	1	375	62.5
5	0.95	356.25	71.25
4	0.91	341.25	85.31
3	0.82	307.5	102.5
2	0.73	273.75	136.87
1	0.54	202.5	202.5

The discharge window can be plotted against the percentage based on a 6 hour discharge rate to determine the relationship for available capacity as a percentage (Figure 5-14).

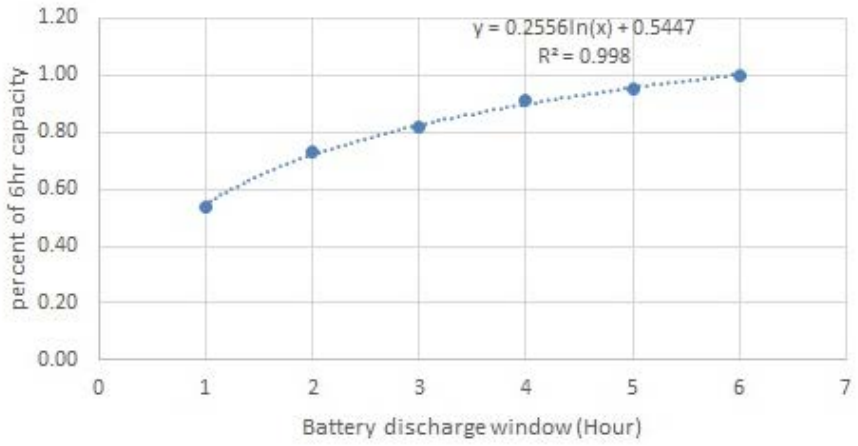

Figure 5-14 Available capacity logarithmic model

Now that the relationship is known, a capacity percentage (Equation 5-2) can be calculated from a given discharge window (t) in hours (Table 5-10). Then, the capacity percentage and the discharge window can be used to calculate the current (amp) draw (Equation 5-3).

$$capacity\% = 0.2556 * \ln(t) + 0.5447$$ Equation 5-2

$$Current(amp) = \frac{capacity\% * battery\_size}{t(h)}$$ Equation 5-3

Table 5-10 Available 40-125-7 capacity using logarithmic model

	discharge window (hours)	Capacity% (decimal)	capacity (Ah)	amp
55min	0.92	0.52	195.92	213.73
50min	0.83	0.50	186.79	224.14
45min	0.75	0.47	176.69	235.58
40min	0.67	0.44	165.40	248.10
35min	0.58	0.41	152.60	261.60
30min	0.50	0.37	137.82	275.65

A linear fit (Equation 5-4) was also considered for the above data. However, the R^2 value for the linear fit (Figure 5-15) was not as good as the logarithmic fit. This linear fit simple battery model is considered a poor choice as the battery state of charge is of importance (Chan, 2000).

$$capacity\% = 0.0871 * t + 0.52$$ Equation 5-4

$$R^2 = 0.9245$$

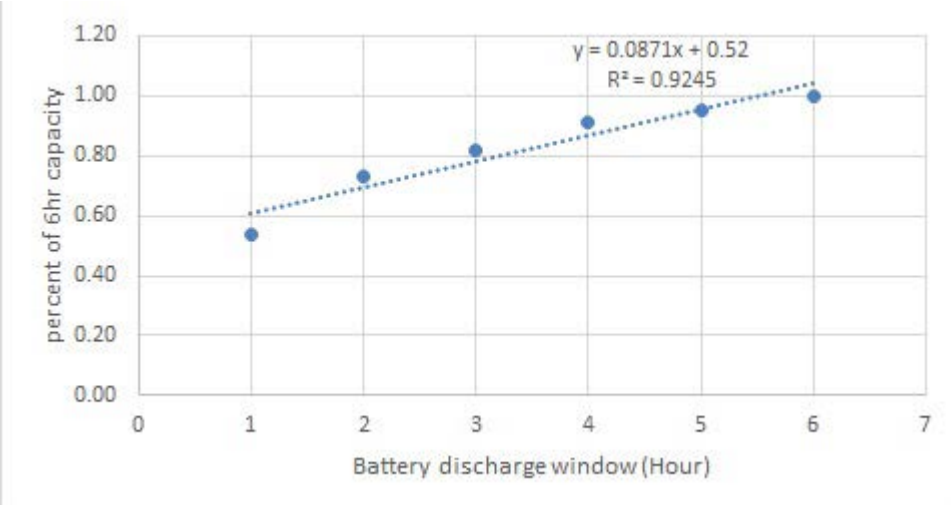

Figure 5-15 Available capacity linear model

A second degree polynomial (Equation 5-5) provided a reasonably good fit. The R^2 value (Figure 5-16) was much better than the linear fit but not quite as good as the logarithmic fit.

$$capacity\% = -0.0161 * t^2 + 0.19968 * t + 0.37 \qquad \text{Equation 5-5}$$

$$R^2 = 0.9916$$

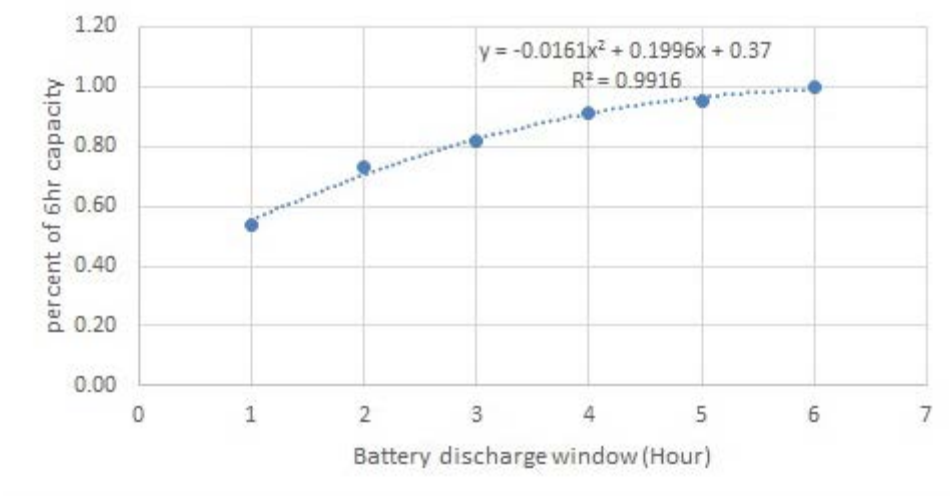

Figure 5-16 Available capacity quadratic model

If the field task requires approximately 214 amps, then the most we can expect from CLARK is 50 to 55 minutes of field work. The finger weeding events recorded on 27 April, 5 June, 7 July, 28 July, 4 September, 16 September (0.5 hours), 9 August (0.5 hours), and 8 October each required less than 50 minutes of field work to complete. CLARK would be expected to fully satisfy this work load without any modification to work schedule. The finger weeding events recorded on 26 May, and on 23 June each required 1.5 hours of work while 15 September required 1.24 hours. If CLARK were charged and ready, then 50 minutes of field work could be performed in the morning allowing CLARK to be charged for 4 to 5 hours upon completion (assuming a longer equalization charge). The remainder of this work could be completed in the afternoon once the battery had been charged. Again, CLARK could be expected to fully satisfy this daily work load with minimal modification to work schedule. Field work on 12 May required 2.05 hours. CLARK would require 3 charges to complete this amount of work. It would be possible to perform this in one long day if the crew chose to do so. Alternatively, this work could be spread over two days. Field work on 12 June required 3.5 hours and 15 August required 3.52 hours. CLARK would require 4 to 5 charges to complete this amount of work. This amount of work would have to spread out over two or three days. Thus, to support finger weeding completely with battery power, the most significant adjustment to field operation scheduling would

require that these two days with heavy finger weeding usage each be spread out over a maximum of three days. It is important to note that significant subsequent finger weeding operations were not required in the three-day window after the days with heavy finger weeding usage. Therefore, this requirement to spread out the operation would not force delays in subsequent operations and the worst-case delay in order to support battery-powered electric finger weeding would be two days. The UK CSA is 12 acres and the recorded finger weeding activity is intended to reflect typical activity on a 12 acre organic vegetable production CSA.

5.4.2 Comment on capacity

A practical comment should be made about the current draw from the Crown battery. As has been mentioned, CLARK utilized a 40-125-7 battery having 375 Ah at 80 VDC. As more current is drawn from the battery, the available capacity diminishes and this behavior has been modeled above (Table 5-10). In addition, the larger the current draw, the more the battery voltage will droop under the load. At approximately 71 VDC the Zapi controllers will perform a system reset assuming the battery voltage is insufficient for the system to perform properly. It is believed this behavior explains the system shutdown captured in the data represented by the above current (Figure 5-6) and voltage (Figure 5-7) plots. A practical limit for this battery coupled with the Zapi controllers is approximately 230-240 amps with a voltage droop to approximately 71-72 VDC. Based on the above, finger weeding at 0.808 m s^{-1} requiring 224 amps and 72.5 VDC is approaching the practical limit of CLARK.

A reasonable way to increase the amount of work CLARK could perform would be to increase the battery capacity. As the size of the battery increases, not only is more total energy available, but more instantaneous power will also be available for power intensive tasks such as plowing. This is reasonable as the current limit of the motors is approximately 300 amps. Possible upgrades for the battery were discussed with Crown including a proposed 80 VDC, 550 Ah battery weighing 1,429 kg (model# 40-110-11). The 40-110-11 dimensions (Height x Width x Depth) of 70 x 101.6 x 73.4 cm were comparable to the 40-125-7 dimensions of 73.7 x 101.6 x 48.2 cm. The 40-110-11 weighed approximately

91 kg more than the 40-125-7 but provided an additional 175 Ah of capacity. The same logarithmic model (Equation 5-2) for available capacity can be applied to the 40-110-11 (Table 5-11).

Table 5-11 Crown 40-110-11 derating information

discharge window (hours)	capacity% (decimal)	capacity (Ah)	amp
6	1	550	91.67
5	0.95	522.5	104.5
4	0.91	500.5	125.12
3	0.82	451	150.3
2	0.73	401.5	200.75
1	0.54	297	297

And, a working time can be estimated for the desired current draw (Table 5-12).

Table 5-12 Available 40-110-11 capacity using logarithmic model

	discharge window (hours)	capacity% (decimal)	capacity (Ah)	amp
100min	1.667	0.68	371.40	222.84
95min	1.583	0.66	364.19	230.01
90min	1.500	0.65	356.59	237.72
80min	1.333	0.62	340.03	255.02
75min	1.250	0.60	330.95	264.76
70min	1.167	0.58	321.26	275.36

With the larger battery, approximately 95 minutes of work could be possible for a task that required 230 amps.

5.4.3 Comment on discharge window and force

The above equations (Equation 5-2, and Equation 5-3) can be used to eliminate the capacity% term yielding (Equation 5-6).

$$\left(\frac{t}{battery\_size}\right) * Current = 0.2556 * \ln(t) + 0.5447 \qquad \text{Equation 5-6}$$

From chapter 4, (Equation 4-11) can be used to remove the current draw and replace it with a desired drawbar force (Equation 5-7).

$$\left(\frac{t}{battery\_size}\right)\left(\frac{F_{DRAWBAR} + 1502}{31.623}\right) = 0.2556 * \ln(t) + 0.5447 \qquad \text{Equation 5-7}$$

This single equation can be used to estimate the discharge window for a given battery size and a desired drawbar force.

If solving the transcendental equation is undesirable, then the above steps can be repeated except using the quadratic model given by (Equation 5-5) instead of the logarithmic model. It is possible to eliminate capacity% using (Equation 5-2, and Equation 5-5) yielding (Equation 5-8).

$$\left(\frac{t}{battery\_size}\right) * Current = -0.0161 * t^2 + 0.19968 * t + 0.37 \qquad \text{Equation 5-8}$$

Replace the current draw with drawbar force using (Equation 4-11) resulting in (Equation 5-9).

$$\left(\frac{t}{battery\_size}\right) * \left(\frac{F_{DRAWBAR} + 1502}{31.623}\right) = -0.0161 * t^2 + 0.19968 * t + 0.37 \qquad \text{Equation 5-9}$$

This equation can be arranged to be in a more desirable form (Equation 5-10).

$$0 = -0.0161 * t^2 + \left(0.19968 - \frac{F_{DRAWBAR} + 1502}{battery\_size * 31.623}\right) * t + 0.37 \qquad \text{Equation 5-10}$$

Equation 5-10 provides a method to solve for one of the three unknowns given information on the other two. If the drawbar force and the duration of a desired operation

are known, then it would be possible to solve for battery size. This enables designing machines targeting certain farm tasks. If the machine were already designed, then the battery size and drawbar force could be used to estimate the duration of time the machine could be used for the chosen task. As an example, consider the 375 Ah battery and a drawbar force of 5265 N. Then (Equation 5-10) becomes (Equation 5-11).

$$0 = -0.0161 * t^2 + (-0.37096) * t + 0.37 \qquad \text{Equation 5-11}$$

This equation can easily be solved graphically or via the quadratic formula to yield t = 0.958 hours (or 57.6 minutes) for these parameters (Figure 5-17).

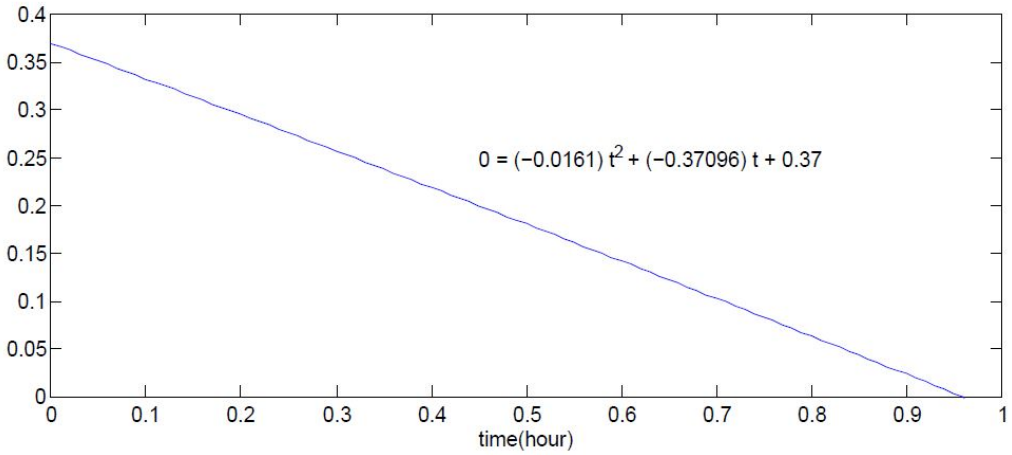

Figure 5-17 Graphical solution for time (h)

5.4.4 Electrical energy balance on a CSA farm

The conventional electric energy needs of a CSA farm and the needs of a fully electric tractor can be balanced by the energy produced from a PV array for an average month (Equation 5-12).

$$PV_{ELECTRIC} - Conventional_{ELECTRIC} - Tractor_{ELECTRIC} = 0$$ Equation 5-12

Where:

$$PV_{ELECTRIC} = Array_{POWER}(kW) * X\left(\frac{peak\_sun\_hours}{day}\right) * 30\left(\frac{day}{month}\right)$$

$$Tractor_{ELECTRIC} = Current(amp) * V(volt) * t\left(\frac{hour}{month}\right)$$

The current can be replaced (using Equation 4-11) resulting in a generalized energy equation (Equation 5-13).

$$Array_{POWER}(kW) * X\left(\frac{peak\_sun\_hours}{day}\right) * 30\left(\frac{day}{month}\right)$$
$$- Conventional_{ELECTRIC} - \left(\frac{F_{DRAWBAR} + 1502}{31.623}\right) * V(volt) * t\left(\frac{hour}{month}\right) = 0$$ Equation 5-13

As already noted, the NREL data (NREL, 2016) suggest that historically an average of 4.5 peak sun hours are available for PV arrays to produce electricity in central Kentucky. Therefore, a 15 kW array is expected to produce 2,025 kWh a month on average (Equation 5-14).

$$15kW * \frac{4.5 peak\_sun\_hours}{day} * \frac{30 day}{month} = \frac{2025 kWh}{month}$$ Equation 5-14

As already noted, the UK CSA used on average 1,134 kWh of conventional electricity each month. The finger weeding data (Table 5-4) indicated that on average CLARK required 15.5 kW of power (214 Amp at 72.5 V) while operating the finger weeder (requiring 5,265 N via Equation 4-11). These values can be substituted into (Equation 5-13) to estimate the hours available each month to perform tasks at this load (Equation 5-15).

$$2025(kWh) - 1{,}134(kWh) - 15.5(kW)t = 0$$
$$\rightarrow t = 57.5(h)$$ Equation 5-15

The monthly maximum of finger weeding reported by the CSA was 5.5 hours for the month of June. Therefore, a monthly energy maximum for CLARK to finger weed the CSA would be approximately 85.25 kWh (Equation 5-16).

$$15.5kW * \frac{5.5hours}{month} = \frac{85.25kWh}{month} \quad \text{Equation 5-16}$$

$$2025kWh - (1{,}134kWh + 85.25kWh) = 805.75kWh \quad \text{Equation 5-17}$$

This implies that on average 805.75 kWh of electricity are available to be sold back to the utility or for additional work each month after accounting for the conventional electric needs and finger weeding (Equation 5-17). If the energy is used for utility tasks similar to finger weeding and with similar energy requirements (15.5 kW), then approximately 52 hours of work are available for additional tasks each month (Equation 5-18).

$$\frac{805.75kWh}{15.5kW} = 52h \quad \text{Equation 5-18}$$

Fifty-two hours available for additional tasks implies that at least 2 full charges are available for use each day of a 20 day work month, as a full charge yields about 55-60 minutes of work at a 214 amp load.

5.5 Conclusions

Electric bills were collected to estimate the monthly average energy need of a 12 acre CSA farm. NREL data were used to estimate the average photovoltaic resource available for central Kentucky. Data for finger weeding events were recorded to determine the distribution in time for these events. Power and energy data were collected for a fully electric tractor and a Kubota L5030 with a custom configuration to match the weight distribution of the electric tractor. A model was developed relating drawbar force, battery size, and the working time at the given force. This model could aid in designing machines targeting certain tasks. Another model was developed to balance the conventional electric energy needs of a CSA farm and the estimated energy needs of a fully electric tractor with the net electric energy produced from a PV array.

A 15kW photovoltaic solar power system could be used to meet the net conventional electric energy needs of a 12 acre diversified organic vegetable production CSA and supply the net energy required for CLARK to meet the CSA finger weeding needs.

- The UK CSA conventional electric need was determined yielding a monthly average of 1,134 kWh.
- Historical NREL data suggests a monthly average photovoltaic resource available for central Kentucky of 4.5 kWh m^{-2} day^{-1}. A 15 kW solar array is expected to produce an average of 2,025 kWh of energy each month according to this data.
- The finger weeding distribution in time for the CSA was determined. Finger weeding operations occurred on 14 days at the UK CSA in 2015. This operation required a daily maximum of 3.52 hours, a weekly maximum of 4 hours, and a monthly maximum of 5.5 hours.
- CLARK required an average power of 15.5 kW to finger weed. In 2015 the annual UK CSA finger weeding need was a total of 17.6 hours. CLARK would require approximately 15.5 kW * 17.6 h = 272.8 kWh of energy to meet this need.

REFERENCES

ASABE. (2015). *Agricultural Machinery Management.* ASAE EP496.3 FEB2006(R2015).

ASABE. (2015). *Agricultural Machinery Management Data.* ASAE D497.4 MAR2011(R2015).

ASABE. (2015). *Uniform Terminology for Agricultural Machinery Management.* ASAE S495.1 NOV2005(R2015).

Average Solar Radiation. (2017, September 05). Retrieved from http://www.pveducation.org/pvcdrom/average-solar-radiation

B.P. Thoreson, R. A. (1986). Electric Choremaster I. *Transactions of the ASAE*.

Borhaug, E., & Pettersen, K. (2005). *Cross-track control for underactuated autonomous vehicles.* 44th IEEE Conference on Decision and Control, and the European Control Converence 2005.

Chan, H. S. (2000). A New Battery Model for use with Battery Energy Storage Systesm and Electric Vehicles Power Systems. *Power Engineering Society Winter Meeting 2000 IEEE.*

Chang, C.-L. Y.-B. (2015). *Integration of Laser Scanner and Odometry for Autonomous Robotics Lawn-mower.* New Orleans, Louisiana: Paper presented at the 2015 ASABE Annual Internation Meeting.

D.C. Slaughter, D. K. (2007). Autonomous robotic weed control systems: A review. *Computers and Electronics in Agriculture*.

diydrones/ardupilot. (2015, December 22). Retrieved from https://github.com/diydrones/ardupilot

diydrones/MissionPlanner. (2015, October 27). Retrieved from https://github.com/diydrones/MissionPlanner

Dybro, N. (2015). *Agronomy Based Crop Production System.* New Orleans, Louisiana: Paper presented at the 2015 ASABE Annyal Internation Meeting.

EPA. (2007). *Inventory of U.S. Greenhouse Gas Emissions and Sinks: 1990-2007.*

Gai, J. T. (2015). *Plant Recogintion through the Fusion of 2D and 3D Images for Robotic Weeding.* New Orleans, Louisiana: Paper presented at the 2015 ASABE Annyal International Meeting.

H.T. Leidenfrost, T. T. (2013). Autonomous Navigation of Forest Trails by an Industrial-Size Robot. *American Society of Agricultural and Biological Engineers*.

Heraud, J. A., & Lange, A. F. (2009). *Agricultural Automatic Vehicle Guidance from Horses to GPS: How We Got Here, and Where We Are Going.* ASABE.

How to Calculate your Peak Sun-Hours. (2016, March 17). Retrieved from https://www.solarpowerauthority.com/how-to-calculate-your-peak-sun-hours/

ISO/ASABE. (2012). *Tractors and machinery for agriculture and forestry - Test procedures for positioning and guidance systesm in agriculture - Part 2: Testing of satellite-based auto-guidance systems during straight and level travel (Vol. 12188-2:2012, pp. 6).* Switzerland: ISO.

Jordan M. Shockley, C. R. (2011). A Whole Farm Analysis of the Influence of Auto-Steer Navigation on Net Returns, Risks, and Production Practices. *Journal of Agricultural and Applied Economics*.

Julius McGee. (2014). *Does certified organic farming reduce greenhouse gas emissions from agricultural production?* Springer Science.

K. Sasaki, M. Y. (1997). Evaluation of electric motor and gasoline engine hybrid car using solar cells. *Elsevier*.

Kentucky Mesonet. (2017, Janurary). Retrieved from www.kymesonet.org

Min Chen, G. A.-M. (2006). Accurate Electrical Battery Model Capable of Predicting Runtime and I-V Performance. *IEEE Transactions on Energy Conversion*.

N. L. Buck, H. A. (1983). Electric Vehicle Desisgns for Agricultural Applications. *American Society of Agricultural Engineers*.

NREL. (2016, July). *Dynamic Maps, GIS Data, & Analysis Tools*. Retrieved from http://www.nrel.gov/gis/solar.html

Oliver Tremblay, L.-A. D.-I. (2007). A Generic Battery Model for the Dynamic Simulation of Hybrid Electric Vehicles. *IEEE*.

Petersen, K., & Lefeber, E. (2001). *Way-point tracking control of ships.* 40th IEEE Converence on Decision and Control.

R. Alcock. (1983). Battery Powered Vehicles for Field Work. *Transactios of the ASAE*.

R. D. Grisso, M. F. (2004). Predicting Tractor Fuel Consumption. *Power & Machinery Division of ASAE*.

Rains, G. C.-P. (2015). *Steps towards an Automonous Field Scout and Sampling System.* New Orleans, Louisiana: Paper presented at the 2015 ASABE Annual International Meegin.

Rodale Institue. (2014). *Regenerative Organic Agriculture and Climate Change.*

Rovira-Mas, F. M.-R. (2015). *Navigation Strategies for a Vineyard Robot.* New Orleans, Louisiana: Paper presented at the 2015 ASABE Annual Internation Meeting.

Sharp, I., & Yu, K. (2012). *Positional Accuracy Measurement and Error Modeling for Mobile Tracking.* IEEE Transactions On Mobile Computing.

US Department of Energy. (2006). *Solar FAQs.* Retrieved from www.sandia.gov: http://www.sandia.gov/~jytsao/Solar%20FAQs.pdf

US Department of Energy. (2017). *About Energy.gov: Mission*. Retrieved from Energy.gov: https://energy.gov/mission

US Energy Information Administration. (2013). *today in energy*. Retrieved from www.eia.gov: http://www.eia.gov/todayinenergy/detail.cfm?id=12251#

US Energy Information Administration. (2017). *About EIA.* Retrieved from www.eia.gov: http://www.eia.gov/about/index.php

Weerachai Arjharn, M. K. (2001). Preliminary Study on the Applicability of an Electric Tractor (Part 1). *Journal of Japanese Society of Agricultural Machinery*.

wiki/Ardupilot. (2016, Janurary 04). Retrieved from https://en.wikipedia.org/wiki/Ardupilot

Williams, A. A. (2006). *Determining the environmental burdens and resource use in the production of agricultural and horticultural commodities: Defra project report ISO205.* Bedford: Cranfield Univeristy and DEFRA.

World Commission on Environment and Development. (1987). *Our Common Future.* Oxford Univeristy Press.

Xi Zhang, M. G. (2010). A semi-autonomous tractor in an intelligent master-slave vehicle system. *Springer-Verlag*.

VITA

Joseph Rounsaville

Educational Institutions Attended and Degrees Awarded

M.S. 2007: University of Kentucky – Physics
M.S. 2001: University of Oklahoma – Electrical Engineering
B.S. 1999: Southeastern Oklahoma State University - Mathematics

Professional Positions

Engineer Associate – University of Kentucky
Test Development Engineer – Hitachi Automotive
Electrical Hardware Engineer – Lexmark International

Professional Publications and Presentations

Rounsaville, J, & Dvorak, J. & Stombaugh, T. *Methods for Calculating Relative Cross-Track Error for ASABE/ISO Standard 12188-2 from Discrete Measurements.* Transactions of the ASABE.

Rounsaville, J, & Dvorak, J. *System Power Requirements for a Fully Electric Drivetrain.* ASABE international meeting, Orlando, FL July 2016.

Joseph Rounsaville

05/17/2017